Biomass Conversion and Biorefinery
https://doi.org/10.1007/s13399-023-04418-z

ORIGINAL ARTICLE

Investigation of the combustion and ash deposition characteristics of oil palm waste biomasses

Fairuz Milkiy Kuswa[1,2] · Hanafi Prida Putra[1,2] · Prabowo[1] · Arif Darmawan[2] · Muhammad Aziz[3] · Hariana Hariana[1,2]

Received: 30 March 2023 / Revised: 26 May 2023 / Accepted: 29 May 2023

Abstract

Biomass serves as an alternative energy solution for decarbonizing coal-fired power plants, which have been reactivated in several countries due to the global energy crisis. Oil palm waste, owing to its abundant availability, holds significant potential as a biomass fuel. This study aimed to investigate the combustion performance of various oil palm wastes in comparison to coal. Biomass combustion is associated with ash-related problems such as slagging, fouling, and corrosion, which may accelerate ash deposit acceleration, reduce heat transfer, and damage refractory equipment in boilers. Ash-related problems were evaluated using the method commonly adopted for solid fuel, including experimental drop tube furnace combustion and ash observation. The results indicate that each oil palm waste has different combustion characteristics. Palm leaves, empty fruit bunch, and palm fronds with clean probe observation have a relatively low tendency of slagging and fouling and can be recommended as biomass fuel for co-firing. However, their high alkali and iron contents need to be considered. Palm fiber has similar combustion characteristics to coal, but it has a high slagging and fouling tendencies. The palm stems with high chlorine content have a high corrosion tendency confirmed by probe observation, scanning electron microscopy, and X-ray diffraction analyses.

Keywords Oil palm waste · Biomass · Combustion · Slagging · Fouling

1 Introduction

Coal has long been the primary fuel for power generation, particularly in densely populated Asian countries like China, India, and Indonesia. As a result of the energy crisis caused by the disruption of gas lines due to the conflict between Russia and Ukraine, several European countries are resorting again to fossil fuels [1]. However, the emission of greenhouse gases, as a consequence of coal burning, can contribute significantly to the acceleration of climate change on a global scale [2, 3]. Research shows that burning coal results in higher levels of carbon dioxide (CO_2), nitrogen oxides (NO_x), and sulfur oxides (SO_x) [4]. These emissions lead to adverse environmental effects, such as acid rain production, the ozone layer's destruction, and the acceleration of global warming [5]. Therefore, it is challenging for nations with significant energy requirements to meet the urgent need to improve environmental quality by reducing their coal consumption. Moreover, following the Paris Agreement, the global community has pledged to implement decarbonization to lower the amount of CO_2 in the atmosphere [6].

It is generally accepted that biomass may be used as a clean and carbon-neutral renewable energy source, which can replace fossil fuels, especially coal [7–9]. Biomass grows by converting the solar energy into chemically stored energy through photosynthesis. Energy from the solar can later be converted into heat and power through combustion. Conceptually, the amount of CO_2 released into the atmosphere is the same as the CO_2 absorbed during the growth of plants. Therefore, this process can be considered carbon neutral [10–12]. Biomass combustion is an intricate process that incorporates many physical and chemical factors. The fuel composition and the intended use of combustion products play significant

✉ Muhammad Aziz
maziz@iis.u-tokyo.ac.jp

✉ Hariana Hariana
hariana@brin.go.id

[1] Mechanical Engineering Department, Sepuluh Nopember Institute of Technology, Surabaya, Indonesia

[2] Research Center for Energy Conversion and Conservation, National Research and Innovation Agency, South Tangerang, Indonesia

[3] Institute of Industrial Science, The University of Tokyo, Tokyo 153-8505, Japan

Published online: 20 June 2023

roles in the combustion process [13]. However, biomass combustion employing co-firing or single fuel still creates issues and complicates the further investigation.

As a tropical country, Indonesia has the advantage of having significantly high biomass potential from agricultural and forestry biomasses. In addition, according to the Index Mundi, Indonesia is the world's largest producer of palm oil commodities, making it a high opportunity to produce green fuels [14–16]. Many parts of oil palm wastes can be recycled and used as material or biomass fuel. Hamada et al. [17, 18] have found that combustion residues from oil palm wastes, such as mesocarp fiber and palm shells, can be used as an aggregate material to obtain a more optimum concrete mix. Several studies [19, 20] have examined the potential of oil palm trees, such as empty fruit bunch (EFB), palm fiber, and palm kernel, as co-firing substitutes in power plants and investigated in terms of power generation and efficiency. Hariana et al. [15] have conducted an in-depth analysis of the co-firing test between coal, EFB, and palm frond to evaluate slagging and fouling tendencies. Moreover, Idris et al. [21] have also discussed co-firing of oil palm waste biomass and coal in terms of emissions.

Agricultural biomass contains larger amount of ash-forming chemicals than woody biomass since it has a rapid metabolic rate and absorbs more nutrients during its growth stage [22]. As shown in the previous study [23], rice husk and oil palm wastes, as agricultural biomass, have a higher composition of silica or potassium, and have higher ash content than woodchip biomass which has a higher composition of calcium. Other studies show the average ash content in wood and woody biomass is around 4.6 wt% compared to agricultural biomass, which is around 8 wt% [24]. Slagging and fouling on the boiler could result from the biomass's high ash content and occur in a two-step mechanism. In the first step, ash particles and vapors make it to the heat exchange surface, where they will deposit. The second step involves the expansion of an ash deposit layer. These two steps can occur sequentially according to the step or together simultaneously [25]. The high alkali metal content also causes slagging and fouling, potentially lowering the sintering temperature of ash [26–28]. Slagging and fouling can reduce boiler efficiency due to the reduced ability for heat exchange. Furthermore, this will cause damage and expensive repair costs [29].

A previous study [15] shows that the combustion of oil palm wastes shows a positive trend; however, at certain proportions, it can cause ash problems. Moreover, several studies only focus on co-firing between coal and EFB, palm frond, and palm kernel shell [15, 19–21, 30], but the combustion behavior of other oil palm wastes like fiber, stem, and leaves is still rare. In order to fill this gap, this study is aimed to investigate and evaluate the combustion aspect of seven different oil palm wastes compared to coal before being implemented for co-firing in existing coal-fired power plants. A lab-scale combustion test was performed utilizing a drop tube furnace (DTF) and thermogravimetric and differential thermal analysis (TG-DTA) to examine the combustion behavior and ash deposit formation. In addition, ash deposits from DTF combustion are further analyzed to find ash-related problem tendencies using scanning electron microscopy–energy dispersive spectroscopy (SEM-EDS) and X-ray diffraction (XRD).

2 Material and methods

Oil palm wastes and coal were analyzed for clarifying their proximate, ultimate, and ash analyses and ash fusion to obtain their characteristics as solid fuel by using coal testing standards. Then, the empirical indices were employed to predict the slagging, fouling, abrasion, and corrosion tendencies of biomasses and coal. TG-DTA was carried out to compare the thermal behavior of biomasses with coal. For the main experiment, a lab-scale DTF combustion test was performed to simulate the slagging and fouling with operating conditions adapted to the actual pulverized coal boiler. During the combustion test, the gas emission was analyzed. The attached ash on the probe surface was observed visually and weighted to find the ash deposit tendency. The ash observation was strengthened with morphological analysis using SEM-EDS and mineral determination using XRD. From the series of tests, each biomass was evaluated and compared to coal as a baseline sample to obtain and clarify the recommended oil palm wastes that have good combustion characteristics with fewer ash-related problems.

2.1 Samples preparation

Seven oil palm wastes were prepared along with one bituminous coal from East Kalimantan, Indonesia. The oil palm wastes consisted of palm fiber, palm leaves, upper stem, middle stem, lower stem, EFB, and palm frond, as illustrated in Fig. 1. The biomass and coal samples were dried (according to ASTM D3302) and pulverized to obtain a size of less than 250 µm for characteristics tests such as proximate, ultimate, calorific value, and total chlorine. For the DTF combustion experiment and thermogravimetric analysis, the coal was pulverized to a particle diameter smaller than 75 µm. On the other hand, the biomass was ground to an average particle diameter smaller than 250 µm after being dried at a temperature of 60 °C for 1 h. The size and preparation were adjusted to pulverized coal boiler feed. The appearance of the pulverized samples used in this study is shown in Fig. 2. Each sample was combusted as a single fuel in the DTF to determine each biomass's combustion behavior, which is further compared to coal.

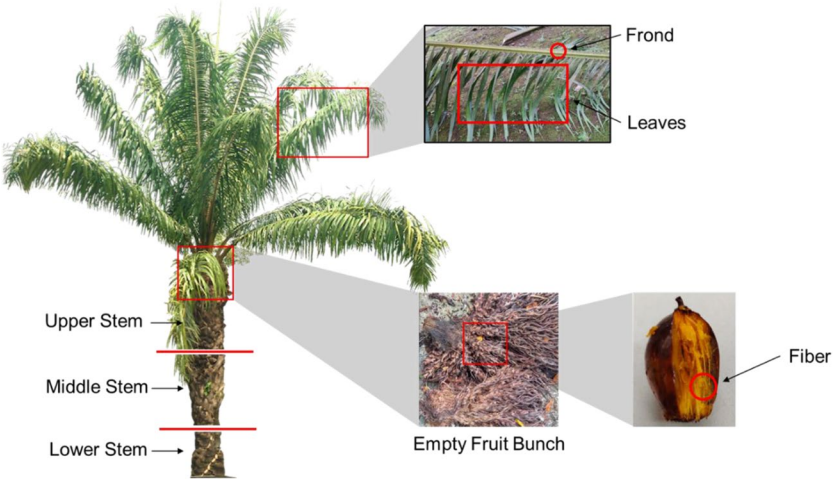

Fig. 1 Part of an oil palm tree

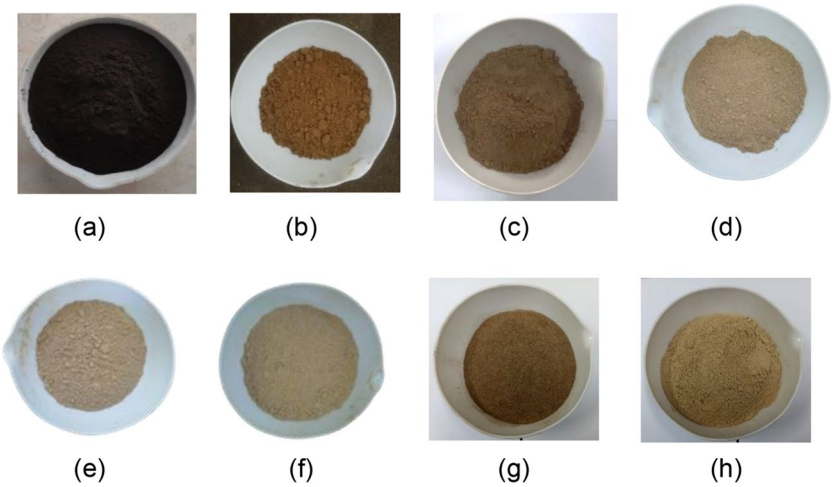

Fig. 2 Powdered samples of (**a**) coal, (**b**) palm fiber, (**c**) palm leaves, (**d**) upper stem, (**e**) middle stem, (**f**) lower stem, (**g**) EFB, and (**h**) palm frond

2.2 Ash fusion temperature (AFT)

The ash melting properties were identified using an ash fusion analyzer equipped with a camera and image processing software to record photos and identify changes from the solid phase to the liquid phase as the temperature rises. These tests followed the conventional procedure for measuring AFTs, and previous investigations have used a similar technique [31, 32]. The sample's ash was shaped into dense pyramids cone and dried. Then, the ash fragments were fixed on ceramic slabs and placed within the ash fusion analyzer's furnace. Regulated gas, with a composition of 60 vol% CO and 40 vol% CO_2, was flown with a flow rate of approximately 1.5 times the furnace volume for the reducing test, while for the oxidizing test, the used gas was regulated air stream. The furnace was heated to a maximum temperature of 1500 °C, and the collected pictures were analyzed to identify the ash's initial deformation (DT), softening (ST), hemispherical (HT), and fluid (FT) temperatures. DT is the temperature at which the initial signs of ash from solid fuel begin to melt. ST is a measure of the clinkering tendency of coal ash and is usually used as a reference where the coal ash in the boiler becomes thicker and sticks to the surface of the boiler. HT is the temperature when the ash shape resembles a hemispherical shape, where the height reaches almost half its initial width. FT is the temperature at which the ash sample is completely fused until the height of the ash approaches the flat surface approximately with a maximum height of 1.6 mm, and only a small portion of the ash does not melt [27, 33].

2.3 Empirical indices of solid fuels

Various studies have relied on the theoretical prediction of coal as a first basis for estimating the likelihood of slagging, fouling, corrosion, and abrasion [26, 34–40]. Theoretical prediction calculation is shown in Table 1. This study used prediction calculations commonly adopted in coal analysis

Table 1 Empirical indices for solid fuels

Parameter	Formula	Low	Medium	High
Slagging indication				
B/A ratio	$\frac{Fe_2O_3+CaO+MgO+Na_2O+K_2O}{SiO_2+Al_2O_3+TiO_2}$	< 0.5	0.5–1.0	> 1.0
Silica ratio	$\frac{SiO_2}{SiO_2+Fe_2O_3+CaO+MgO} \cdot 100$	> 72	65–72	< 65
Fusibility	$\frac{(4\ x\ DTreducing)+HToxidizing}{5}$	> 1343	1232–1343	<1232
Composite index	$1.24\frac{B}{A} + 0.28\frac{SiO_2}{Al_2O_3} - 0.0023ST$ $-0.019\ Sr + 5.4$	< 1.5	1.5–2.5	> 2.5
Slagging index	$\frac{B}{A}.S$	< 0.6	0.6–2.0	> 2.0
Iron in ash	Fe_2O_3	<8.0	8.0–15.0	> 15.0
Fouling indication				
Fouling index	$\frac{B}{A}.(Na_2O)$	< 0.2	0.2–0.5	> 0.5
Sodium in ash	Na_2O	< 2.0	2.0–6.0	> 6.0
Total alkali	$Na_2O + K_2O$	< 2.0	2.0–3.0	> 3.0
Abrasion indication				
Abrasion index	$qc + 0.5\ pc + 0.2\ Ash$ $qc = 0.01xAshx(SiO_2 - 1.5Al_2O_3)$ $pc = 1.3x(Sulfur - 0.3)$	< 4.0	4.0–8.0	> 8.0
Corrosion indication				
Sulfur/chlorine	$\frac{S}{Cl}$	> 4.0	2.0–4.0	< 2.0

with justified parameters for the biomass samples in oil palm waste.

2.4 Combustion characteristics using TG-DTA

The thermogravimetric analyzer was used to obtain the combustion characteristics of solid fuels. Shimadzu DTG-60 was utilized in the atmospheric environment to carry out the analysis. Samples weigh approximately 8–10 mg and were heated from ambient temperature to 800 °C at a rate of 10 °C/min. The temperature was held for 10 min at the final temperature.

2.5 Combustion of solid fuels in DTF

DTF testing has been carried out in several recent studies [38, 41–43] to find the tendency of slagging and fouling in power plants, especially in pulverized coal boilers. The DTF has been demonstrated in the previous study [41]. A ceramic tube was made of alumina with a length of 1.5 m and an outer diameter of 76.2 mm. The tube was placed in a chamber heated by 1-kWth electric heaters with a temperature range of 1200 to 1250 °C using a convection heating system. In addition, the solid fuel was fed at a rate of 50 g/h via primary air heated at 100–150 °C. Secondary air was added to the combustion chamber to ensure perfect combustion with 3–5% excess oxygen. Exhaust gas measurements were carried out at the bottom of the DTF using a portable gas analyzer Bacharach PCA-400. SO_2 and NOx emissions were measured following the quality standards of the Indonesian Ministry of Environment (KLHK). The gas analyzer was corrected to 7% O_2 concentration using an equation from Li et al. [44] to meet the requirements of the Indonesian government policy.

Furthermore, the ash formed during the combustion was collected from a probe having a diameter of 50 mm (shown in Fig. 3) located at the end of DTF. The probe was inserted, and the height was adjusted so that the temperature sensor on the probe surface showed a temperature of 550 and 600 °C. These temperature conditions simulate slagging and fouling areas in the superheater and economizer areas in the boiler.

After 1 h of residence time, the probe was removed from DTF. The ash collected on the probe surface was weighed to determine the ash deposit weight. The ash was brushed, and the remained ash attached to the probe surface was visually examined following the method of Ohman et al. [45]. Category 1 indicates that the ash adhering to the probe does not coalesce and sinter to the probe's surface. The ash can break with only a light touch. Category 2 means that some ashes adhere to the surface of the probe, but this ash can also break with a light touch. Category 3 indicates that the ash is sintered and adhered with the probe's surface to form small material slag, which is still breakable using one bare hand. Category 4 is ash that sticks and sinters with the surface of the probe to become a more extensive slag material that is not easily broken with one bare hand.

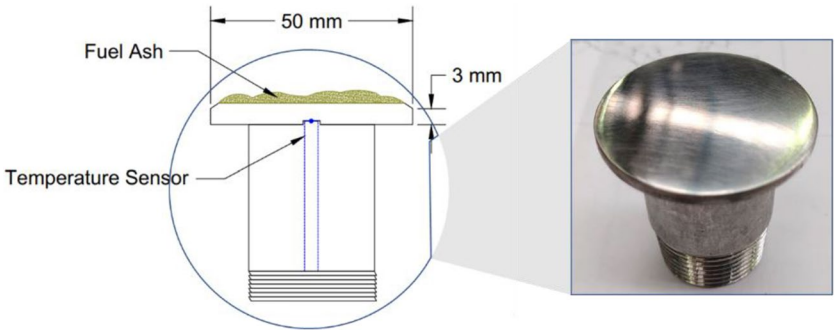

Fig. 3 Testing probe with stainless steel material

2.6 Ash mineralogy characteristics

Ash from DTF combustion was analyzed by SEM-EDS using Quanta 650 and XRD using an Aeris-type Bragg-Brentano Diffractometer to characterize ash's microstructural and minerals. Backscattered electron imaging (BSE) and EDS were utilized in this investigation to analyze the fly ash samples. BSE are electrons that have high energy directly reflected from the surface of the object being tested with differences in grayscale intensity between the chemical phase of an object. On the other hand, the EDS detector could identify elements with an atomic number [46]. XRD was performed with Cu as the X-ray source and angle measurement from 10 to 90° with a 0.02° measurement step. Then XRD pattern was analyzed using MAUD to obtain the minerals composition in ash.

3 Results

3.1 Solid fuel analysis

Initial analysis for solid fuel characterization is very important for energy calculations and early prediction of problems in a power plant [47]. All results of the proximate and ultimate analysis are on a dry basis (db) except for moisture content and calorific value (Q_{gr}) on an as-received basis (ar), as shown in Table 2. The moisture content of the stem samples is relatively high compared to other biomass, especially the middle stem (65.22 wt%), since the stem stores more food reserves in the form of water [48]. The moisture possessed by palm fiber and palm leaves is relatively low compared to coal. The lowest moisture content is owned by palm fiber (8.43 wt%), making it have a high as-received calorific value (Qgr_{ar}). The combination of high moisture content and particle size of biomass injected in the pulverized boiler may result in delayed combustion and lower peak flame temperatures [49]. The ash content of palm leaves is the highest compared to coal and other oil palm wastes. The order of the ash content from the highest to the lowest is as follows: palm leaves > coal > upper stem > palm fiber > middle stem > EFB > lower stem > palm frond. This is probably due to the large amounts of Si and Fe, which play a role in ash deposit formation. The high composition of Si in biomass tends to produce more ash deposit [39]. Moreover, a high alkali composition (Na and K) in palm leaves can form low eutectic alkali-aluminosilicate [40]. In addition, a high Fe composition on palm leaves can accelerate ash deposit formation because of its low melting point [50].

The volatiles owned by biomass appear to be more dominant than coal, corresponding to the lower fixed carbon content in biomass. Moreover, certain ash-forming elements in biomass can increase volatilization and hazardous component [22]. The calorific value of biomass is relatively lower than coal [15, 51]. Only palm fiber has an as-received calorific value close to coal with a value above 4000 kcal/kg. Three parts of the stem (upper, middle, lower) have a very low calorific value, ranging only from 1500 to 1800 kcal/kg in Qgr_{ar}. This is due to the high moisture content possessed by the palm stem. This is also evident in EFB and palm frond, which also have calorific values under 3000 kcal/kg due to their high moisture content. However, when moisture on biomass is removed, the heating value of the biomass has a relatively similar value above 4000 kcal/kg in the following order: palm fiber > palm leaves > EFB > palm frond > lower stem > middle stem > upper stem.

The chlorine content in biomass shows a larger value than in coal. Moreover, palm stem has a very high chlorine value compared to palm leaves, palm fiber, EFB, and palm frond, which has chlorine value under 3000 ppm. Fly ash tends to condense in superheaters because of chlorine, which allows for developing low-melting eutectics and chlorides. By reacting with the alkali in the biomass, the chlorine will further precipitate on the heating surface and react with the metal surface's protective oxide layer, thereby triggering corrosion [26, 52, 53].

Elements present in biomass ash, like potassium and chlorine, can cause low AFTs and produce low-temperature and low-viscosity melting ash, which leads to slagging, fouling, corrosion, and abrasion [22, 54, 55]. The elements in the ash of all samples that are the subject of this study are shown in Table 2. The richest SiO_2 content is found on the upper stem compared

Table 2 Coal and oil palm waste biomass characteristics

Samples	M_{ar} (wt%)	Ash_{db} (wt%)	VM_{db} (wt%)	FC_{db} (wt%)	C_{db} (wt%)	H_{db} (wt%)	N_{db} (wt%)	O_{db} (wt%)	S_{db} (wt%)	Qgr_{ar} (kcal/kg)	Qgr_{db} (kcal/kg)	$Chlorine_{db}$ (ppm)
Coal	25.55	8.65	42.99	48.36	66.79	3.65	1.42	18.63	0.87	4889	6566	191.31
Palm fiber	8.43	5.09	75.95	18.95	51.42	5.09	0.72	37.54	0.14	4313	4762	1766.60
Palm leaves	18.05	14.28	67.46	18.26	46.03	4.23	2.30	32.96	0.20	3636	4437	2597.76
Upper stem	63.04	6.19	73.81	20.00	45.82	4.14	2.15	41.55	0.15	1505	4071	4590.31
Middle stem	65.22	4.83	75.73	19.44	46.35	2.90	0.69	45.10	0.14	1475	4241	4808.24
Lower stem	57.94	2.32	80.27	17.41	47.78	4.43	0.29	45.13	0.05	1834	4362	4559.66
EFB	56.63	3.36	78.34	18.30	47.65	5.31	0.65	42.94	0.08	1902	4385	1523.27
Palm frond	48.13	2.22	82.61	15.17	47.11	5.16	0.49	44.92	0.11	2272	4381	1577.66

M moisture, *Ash* ash content, *VM* volatile matter, *FC* fixed carbon, Qg_r gross calorific value, *ar* as-received, *db* dry basis

to coal and other biomass. Silica has a good effect because its high melting point can raise the AFT [52, 56]. On the other hand, Zevenhoven et al. [57] explained that the interaction between high Si and K in biomass, especially agricultural-based, can cause severe ash-related problems during combustion due to the low melting point of K-silicate. This compound adheres with other particles to form slag in the boiler.

Table 3 shows the results of ash analysis of coal and oil palm waste biomasses. Coal samples, followed by palm leaves, own the highest Al_2O_3 content. In contrast, palm stems in all biomass parts had the lowest Al_2O_3 content. Generally, aluminum in biomass may be in the form of aluminosilicates when impurities are present. The high value of aluminosilicates may increase the AFT and react to capture the alkaline vapor during combustion [52]. Palm frond samples contain more Fe_2O_3 and CaO than other biomass; this poses a risk to the boiler due to the low melting point, and it will result in slagging when exposed to temperatures above a certain threshold [58, 59]. Besides that, the largest amount of MgO is owned by the palm frond and the lower stem. MgO may improve the combustion characteristics and mitigate slagging and fouling in the boiler [60]. Overall, oil palm waste biomass has a lower composition of Na_2O and SO_3 than coal. However, it cannot be denied that the potassium (K_2O) content in this oil palm waste is normally greater than coal, especially EFB, which can lower ash melting temperature.

The solid phases of biomass and coal ash may react with one another to generate minerals or liquid phases when heated [61, 62]. As shown in Fig. 4, coal has a fairly good AFT (with a DT of 1190 °C) with medium slagging and fouling tendency [37]. Deformation value means the temperature at which ash begins to melt, then proceed with the softening temperature, which indicates a change in the ash becoming a liquid phase. Line graphs in Fig. 4 that coincide with coal are palm frond and palm fiber samples, which means these two samples have similar characteristics close to coal in the AFT aspect. Palm frond and palm fiber also have a medium tendency of slagging and fouling because the range of their DT is between 1100 and 1300 °C [63]. Palm frond, which has a medium tendency, has the second highest DT value of 1240 °C influenced by the highest MgO content of 12.89 wt% compared with other biomass [15]. High MgO leads to the production of high melted particles, which result in high AFTs [2, 60]. Palm fiber has high SiO_2 and Al_2O_3 content that cause medium AFT with DT value at 1140 °C. Palm leaves are the samples with the highest DT, reaching 1305 °C, making them have the lowest tendency of slagging and fouling [63]. It is probably influenced by lower potassium and higher Al_2O_3 contents in palm leaves [26].

The lower stem has a higher AFT than the middle and upper stems because of a higher MgO content, which is a

Table 3 Ash analysis of coal and oil palm waste biomasses

Samples	Ash analysis (wt%)										
	SiO_2	Al_2O_3	Fe_2O_3	CaO	MgO	TiO_2	Na_2O	K_2O	Mn_3O_4	P_2O_5	SO_3
Coal	55.70	17.12	8.92	4.50	3.36	0.89	2.09	2.12	0.06	0.43	4.52
Palm fiber	60.05	10.00	2.56	9.13	5.91	0.18	0.18	10.02	0.18	0.18	0.12
Palm leaves	51.93	12.90	11.05	10.22	2.79	0.14	2.83	2.95	0.83	1.78	2.27
Upper stem	72.80	5.02	1.08	4.46	3.82	0.05	0.18	11.07	0.16	0.10	0.18
Middle stem	57.26	8.78	4.61	7.37	7.69	0.12	0.19	13.15	0.27	0.10	0.18
Lower stem	50.06	7.63	4.85	10.00	11.16	0.09	0.19	14.85	0.35	0.10	0.21
EFB	33.85	1.61	5.44	7.28	5.01	0.08	0.40	32.58	0.09	4.23	2.03
Palm frond	22.03	1.80	28.59	19.72	12.89	0.23	0.38	5.58	0.18	2.27	2.62

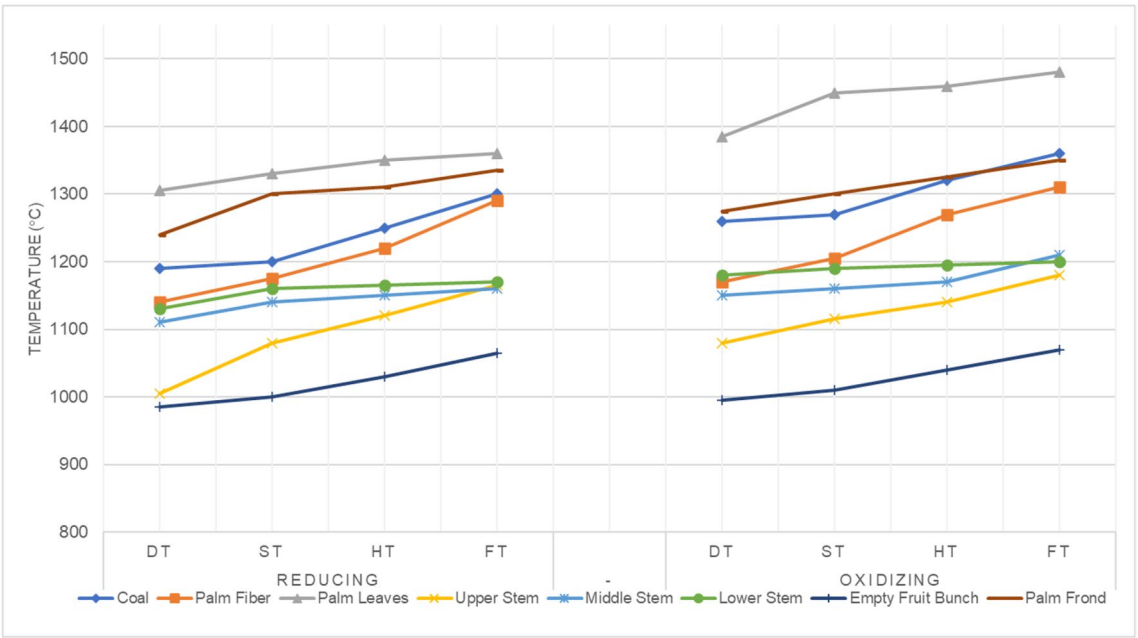

Fig. 4 AFT comparison of coal and oil palm wastes

similar case to the high AFT of the palm frond. As can be observed, the ash fusion temperatures (DT, ST, and HT) can be ordered as follows: upper stem < middle stem < lower stem, while the FT of those three samples shows similar values. The upper stem has a high slagging and fouling tendency due to low DT, below 1100 °C, while the others show a medium tendency. The lowest AFT of all biomasses is shown by EFB, with a DT of below 1000 °C, due to higher contents of K_2O and CaO, which can decrease the solid fuel ash melting temperature [26]. EFB has the highest potential of melting ash, which can react with hazardous components such as chloride and then accommodate slagging and fouling in the boiler area [26, 34].

3.2 Theoretical prediction of samples

Table 4 shows the scores for determining the tendency range for several parameters. Green highlights indicate low tendency, with a score point of 0.0; yellow highlights indicate medium tendency, having a score point of 0.5; and red highlights indicate high tendency, with a score point of 1.0. The slagging parameters (a total of six parameters) are considered to show a high slagging tendency if the total score of slagging is > 3.5, a medium slagging tendency if the total score is 2.5–3.5, and a low slagging tendency if the total score is < 2.5. Likewise, the fouling parameters (a total of three parameters) are considered to have a high fouling

Table 4 Calculated and predicted indexes of coal and oil palm waste biomass

Parameter	Coal	Palm Fiber	Palm Leaves	Upper Stem	Middle Stem	Lower Stem	EFB	Palm Frond
B/A Ratio	0.28	0.40	0.46	0.26	0.50	0.71	0.86	1.10
Silica Ratio	76.85	77.33	68.34	88.61	74.43	65.81	68.86	44.11
Fusibility	1216	1166	1336	1032	1122	1143	1112	1271
Composite Index	2.44	3.52	2.74	5.62	3.81	4.20	3.89	3.86
Slagging index	0.24	0.06	0.09	0.04	0.07	0.03	0.16	0.12
Iron in ash	8.92	2.56	11.05	1.08	4.61	4.85	6.06	8.97
Total Slagging	***2.0 out of 6.0***	***2.0 out of 6.0***	***2.5 out of 6.0***	***2.0 out of 6.0***	***2.0 out of 6.0***	***3.0 out of 6.0***	***3.0 out of 6.0***	***4.0 out of 6.0***
Fouling Index	0.6	0.07	1.30	0.05	0.09	0.13	0.40	3.26
Sodium in ash	2.09	0.18	2.83	0.18	0.19	0.19	0.47	2.97
Total Alkali	0.27	10.20	5.78	11.25	13.34	15.04	23.81	5.97
Total Fouling	***2.0 out of 3.0***	***1.0 out of 3.0***	***2.5 out of 3.0***	***1.0 out of 3.0***	***1.0 out of 3.0***	***1.0 out of 3.0***	***1.5 out of 3.0***	***2.5 out of 3.0***
Abrasion index	4.21	2.98	6.70	4.52	2.36	1.03	2.71	1.03
Total Abrasion	***0.5 out of 1.0***	***0.0 out of 1.0***	***0.5 out of 1.0***	***0.5 out of 1.0***	***0.0 out of 1.0***	***0.0 out of 1.0***	***0.0 out of 1.0***	***0.0 out of 1.0***
Corrosion index	40.90	0.71	0.69	0.29	0.26	0.09	0.50	0.61
Total Corrosion	***0.0 out of 1.0***	***1.0 out of 1.0***	***1.0 out of 1.0***	***1.0 out of 1.0***	***1.0 out of 1.0***	***1.0 out of 1.0***	***1.0 out of 1.0***	***1.0 out of 1.0***

Tendencies : *Low* *Medium* *Severe*

tendency if the total score of fouling is > 2.5, a medium fouling tendency if the total score is between 1.5–2.5, and a low fouling tendency if the total score is < 1.5.

As shown in Table 4, palm fiber, upper stem, and middle stem show a low slagging tendency with a total score of 2.0 out of 6.0, similar to coal with different high-tendency slagging parameters. Coal, palm fiber, upper stem, and middle stem have the same high tendency in fusibility but different composite indexes.

Meanwhile, the other biomasses have a medium to high slagging tendency. Furthermore, a striking parameter difference is found in the B/A ratio, which is owned by coal, palm fiber, palm leaves, upper stem, and middle stem, which tend to have a lower tendency than other biomass, which means these five samples have less base content than the other samples.

Palm fiber and stems show a low fouling tendency with a tendency score of 1.0 out of 3.0 due to lower Na_2O content. Na_2O content in ash is used in all fouling indices and become an important fouling indicator [64]. Moreover, Na_2O has a low melting point below 1200 °C, which is lower than the furnace temperature. In addition, K_2O also needs to be considered because of its low melting point (700 °C) [24]. Coal, palm leaves, and palm frond have a high tendency of fouling compared to other biomass. However, coal still has a lower total alkali content than all palm biomass samples. For the abrasion parameter, only coal, palm leaves, and upper stem have a medium tendency, while other samples have a low tendency. In the aspect of corrosion, only coal has a low tendency from the S/Cl ratio, while all biomass has a high tendency due to the high chlorine value of the biomass.

3.3 Combustion characteristics

From the results of the TGA, the basic combustion parameters are shown in Table 5, followed by the thermogravimetric (TG) and thermogravimetric derivatives (dTG) of the coal and palm-based biomass samples in Fig. 5. The ignition temperature (T_{ig}), which means material ignition spontaneously triggered by external heat [65], shows that palm biomass has a lower value than coal according to the steepness of the TG graph. T_{ig} of coal is higher (341 °C)

Table 5 Combustion parameter obtained from TG-DTA

Samples	T_{ig} °C	T_{bo} °C	T_{bo}-T_{ig} (T_q) °C	T_{max} °C	R_{max} mg/s
Coal	341.00	561.20	220.20	394.30	0.01
Palm fiber	302.28	487.23	184.95	353.48	0.08
Palm leaves	247.16	482.55	235.39	369.95	0.08
Upper stem	248.81	458.65	209.84	312.29	0.04
Middle stem	292.67	387.00	94.33	321.59	0.10
Lower stem	272.94	407.29	134.35	325.88	0.12
EFB	233.44	389.19	155.75	335.98	0.13
Palm frond	258.64	365.67	107.03	336.42	0.13

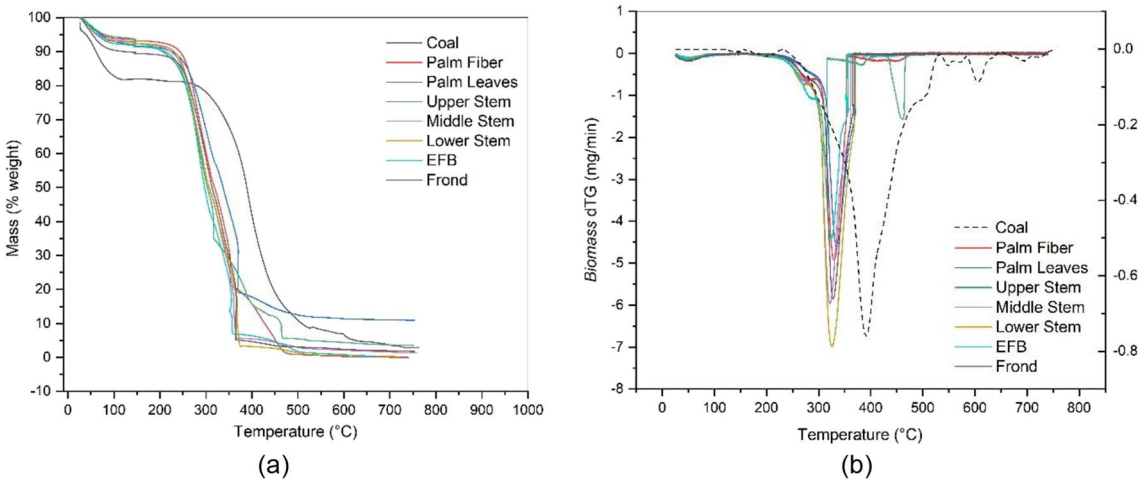

Fig. 5 (**a**) TG and (**b**) dTG curves of coal and biomass samples

than all of the biomass with a range of 200–300 °C due to very low volatile matter compared to biomass [23, 66]. Biomasses had lower T_{max} values than coal, meaning that biomass has higher reactivity than coal. It also relates to R_{max} as the maximum combustion rate. Biomass has a relatively high combustion rate compared to coal, which only has a maximum combustion rate of 0.01 mg/s. It means that biomass is easier to be ignited and combusted than coal. For burnout temperature (T_{bo}), which means the final combustion of material to be burned out where in the TG curve (Fig. 5), the heat flow rate is 0, the palm frond has a very low T_{bo} value compared to other biomass, and the T_{bo} value in coal is the highest. The difference in value between T_{bo} and T_{ig} means the necessary time for the material to be burned out. The middle stem is biomass with the lowest $T_{bo} - T_{ig}$ compared to other biomass, meaning the middle stem takes a shorter time to be burned out [67].

Coal has a volatile decomposition phase and a char in one peak decomposition phase, which starts at a temperature of 250–530 °C, so it can be said that the combustion of volatile matter and char in coal occurs sequentially. In the coal sample, there are small peaks after the main peak, indicating char residue combustion until the material mass is completely used up [65]. Biomass usually consists of two stages, where the first stage is the decay of hemicellulose and cellulose, and the second stage is the decay of lignin, residual volatiles, and char [65, 68]. Palm fiber, middle stem, lower stem, palm frond, and EFB have similar curves from oil palm biomass. The first stage occurs at a temperature of 250–300 °C and the second at a temperature of 300–375 °C. The two stages in palm leaves become one with a temperature range of 250 to 375 °C. Meanwhile, the first upper stem stage occurs at a temperature of 250–330 °C and the second stage at 430–460 °C.

3.4 Qualitative probe observation

Figure 6 shows that the ash deposits on the probe have been brushed, and the probe surface has been observed qualitatively [45, 69]. As can be observed, coal combustion shows the cleanest probe compared with all biomass combustion. This ash probe sample can be categorized as category 1. The partly and sintered ash categories 2 and 3 can be found in all biomass samples. EFB is a biomass that produces a cleaner probe than other biomass and is categorized as category 2, both at probe temperatures of 550 and 600 °C. Ash, which is sintered on the probe, can be removed easily with a light touch. Palm leaves and palm fronds are categorized as category 3. Visualizing this probe looks like some sintered ash is attached to the probe's surface. The remaining material was very difficult to remove but could still be removed with some firm pressure by hand. Sintered ash, categorized as category 4, is visible in the case of a palm fiber sample at a probe temperature of 550 °C; the remaining material on the surface of the probe is very difficult to remove and completely fused with stainless steel material on the probe. However, this fused slagging material was not found in the case of the palm fiber sample at a probe temperature of 600 °C. The appearance of the probe, which looks very corrosive with ash adhered to the probe surface, is found in the palm stem sample in all parts, both upper, middle, and lower.

Figure 7 shows ash deposits weight from 1-h combustion in DTF. However, it is possible that the ash component in samples such as K_2O, Na_2O, SiO_2, and Fe_2O_3 also causes a lot of ash deposits in combustion. A large amount of ash owned by the upper and middle stem results from high silica, potassium, and chlorine content. A high alkali metal and silica content with low deformation temperature can be a prefix for ash deposition on hot surfaces at low temperatures

Fig. 6 Probe observation

and then accommodate slag material which inhibits boiler heat transfer [70, 71]. In contrast, the lower stem, which is rich in potassium, has a low ash deposit due to low ash, high SiO2, and high MgO compared to the other two parts of the stem. Coal with high SiO_2 and Al_2O_3 values results in low ash deposits below 0.1 g. Likewise, low ash was found in palm fiber, lower stem, and EFB. Palm fiber with 60.05 wt% SiO_2 and 10 wt% Al_2O_3 had a positive impact on the formation of ash deposits [72]. Meanwhile, EFB with low ash content produces low ash deposits even though it has high K_2O. Palm leaves and palm fronds have a relatively high ash deposit due to the high content of Fe_2O_3 and CaO, where these two elements play an important role in the formation of ash deposits [50, 73].

3.5 Emission from DTF combustion

Based on gas emission analysis on coal and oil palm wastes, the O_2 value in the exhaust gas ranged from 3 to 5%, and the CO_2 value obtained was not significantly different. Coal has a CO_2 value of 16.1%, and biomass has a CO_2 value of around 15%, as shown in Fig. 8a, except for the EFB and

Fig. 7 Ash deposition

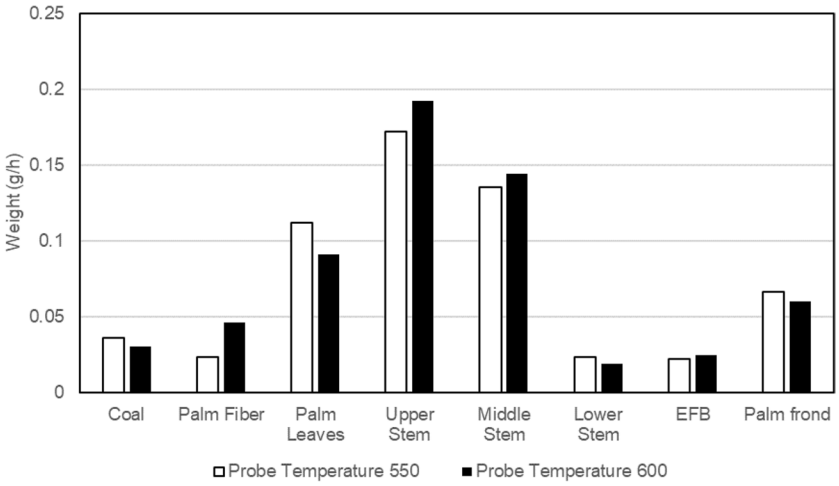

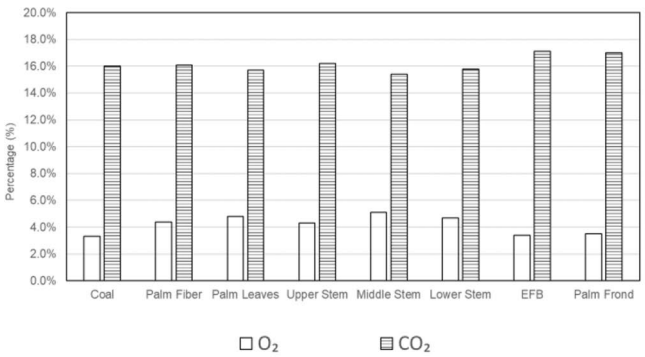

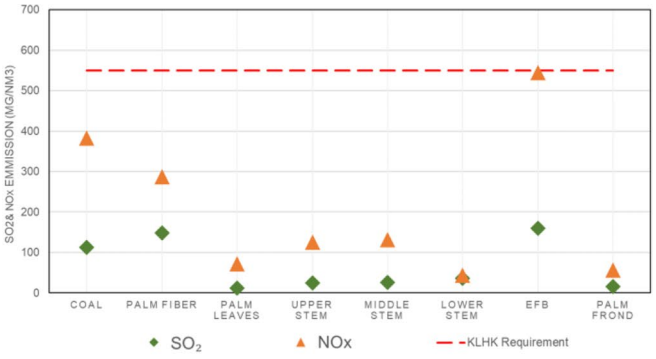

Fig. 8 (**a**) Mean value of excess oxygen and CO_2 from DTF; (**b**) SO_2 and NO_X emissions @ O_2 7%

palm frond samples, which have a higher CO_2 value of 17%. Generally, the carbon content of the fuel affects the value of CO_2 in the combustion products; additionally, the value of volatile matter can affect the exhaust gas CO_2, which can influence the rate of volatilization of the results of fuel combustion, which is higher in the gas phase than the formation of char. [74, 75].

As shown in Fig. 8b, the coal sample showed SO_2 values of 112.4 mg/Nm^3, higher than oil palm wastes except for palm fiber and EFB, which have values of 148.68 and 160.04 mg/Nm^3, respectively. Sulfur in coal and biomass is composed of organic and inorganic components formed during the devolatilization phase. The lack of excess air in the combustion process affects the high sulfur dioxide value formed [76, 77]. The sulfur content of palm fiber is relatively high, consistent with the extra air present during combustion. The NO_x emission of coal is relatively high, with a value of 382.35 mg/Nm^3, consistent with the high nitrogen content of the coal sample compared to the biomass sample. In contrast, almost all of the oil palm waste samples had lower NO_X levels except EFB, which had a higher NO_X value than the coal sample (544.88 mg/Nm^3). However, the high NO_x value in the EFB sample is probably due to the volatile matter's influence. Kim et al. and Y. Lin et al. [74, 75] have also confirmed that NO_x is released at volatile combustion temperatures. That is similar to the increased CO_2 emission caused by the volatile matter in biomass combustion.

3.6 SEM-EDS analyses

The SEM results of the ashes from the combustion of samples with two different probe temperatures using DTF are shown in Figs. 9, 10, 11, 12, 13, and 14. The color spectrum in morphological SEM is also presented to ease the observation of elements contained in morphological images and is supported by the percentage of elemental composition using EDS.

Figure 9a and b are the morphology of the coal sample as a reference. As can be observed, the particles contained in this sample are dominated with a size of 50–100 µm. Particle C (Fig. 9b) is a spherical shape with a bright color observed

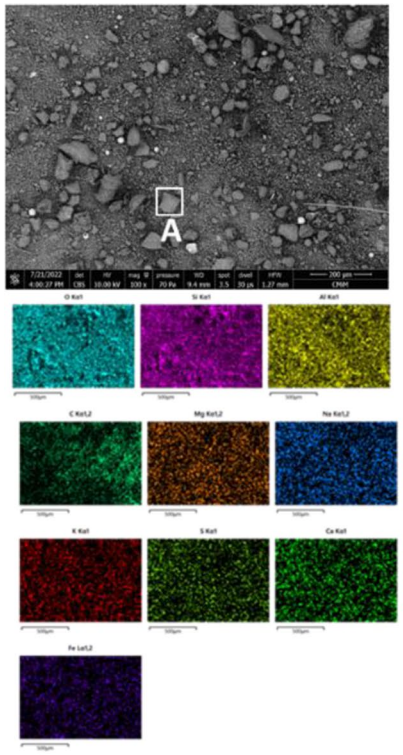

Component (%weight)	
O	39.50
C	25.30
Si	16.50
Al	9.20
Fe	3.90
Ca	1.70
K	0.90
S	0.90
Mg	0.70
Na	0.70

(a)

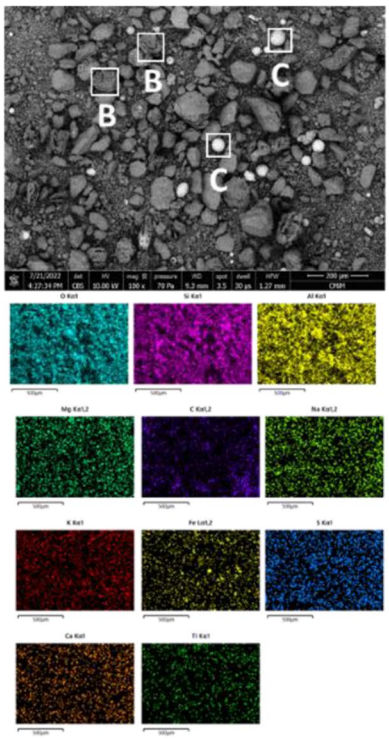

Component (%weight)	
O	43.00
C	11.80
Si	22.60
Al	11.20
Fe	5.20
Ca	1.20
K	2.20
S	0.60
Mg	0.90
Na	0.70
Ti	0.60

(b)

Fig. 9 Morphology and elemental analysis results of coal samples: (**a**) probe temperature of 550 °C and (**b**) probe temperature of 600 °C

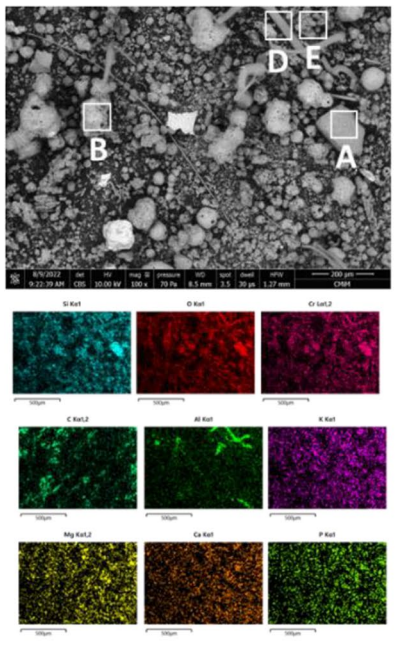

Component (%weight)	
O	35.10
C	24.80
Si	18.30
Al	2.70
Fe	2.90
Ca	3.90
K	6.10
S	0.60
Mg	1.70
Na	0.30
Cr	2.40
P	1.30

(a)

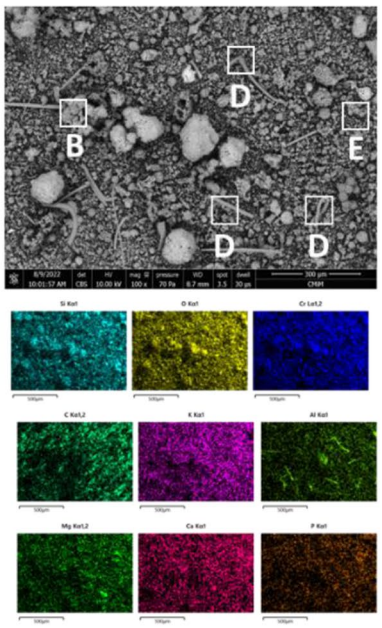

Component (%weight)	
O	32.50
C	26.90
Si	14.70
Al	2.50
Fe	2.40
Ca	5.50
K	7.00
S	0.60
Mg	2.30
Na	0.20
Cr	3.50
P	1.80

(b)

Fig. 10 Morphology and elemental analysis results of palm fiber samples: (**a**) probe temperature of 550 °C and (**b**) probe temperature of 600 °C

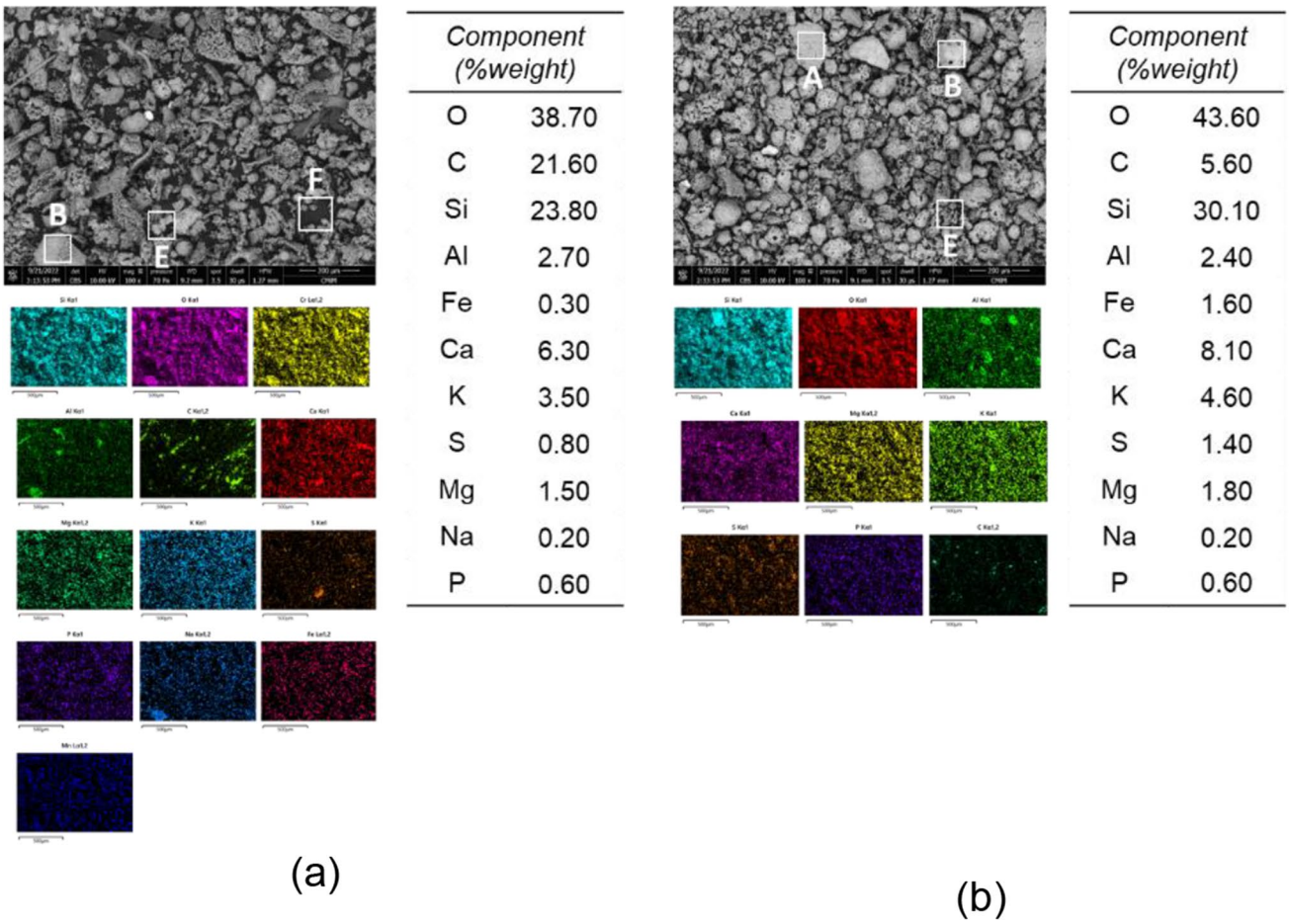

Component (%weight)	
O	38.70
C	21.60
Si	23.80
Al	2.70
Fe	0.30
Ca	6.30
K	3.50
S	0.80
Mg	1.50
Na	0.20
P	0.60

Component (%weight)	
O	43.60
C	5.60
Si	30.10
Al	2.40
Fe	1.60
Ca	8.10
K	4.60
S	1.40
Mg	1.80
Na	0.20
P	0.60

Fig. 11 Morphology and elemental analysis results of palm leaves samples: (**a**) probe temperature of 550 °C and (**b**) probe temperature of 600 °C

at the probe temperature of 600 °C. It looks more numerous compared to the probe temperature of 550 °C. This particle represents heavy metal in the form of iron oxides which melt during combustion [78]. According to EDS results, the percentage of Fe at a probe temperature of 600 °C has a portion of 5.2 wt%, while at a probe temperature of 550 °C, it only has a value of 3.9 wt%. Powdered dry shape with fine particles below 10 µm, which are harmless and usually fall off easily into bottom ash in boilers [79], looks more dominant at a probe temperature of 550 °C. Particles with shapes of smooth surfaces and sizes above 100 µm (particle A) are observed. It means the particle has a high melting point and retains its original shape when fired, representing the elements Si and Al. Particle B is an amorphous particle that does not melt during combustion. It is similar to particle A in ash chemistry but with alkaline minerals condensed on its surface [79].

Figures 10, 11, 12, 13, and 14 are the morphological result for the sample biomass. As shown in Fig. 10, many shapes measure up to 100 µm with smooth surface shapes, such as particle A. Moreover, based on the morphological analysis, tubular particles, such as particle D, which is aluminum oxide, seem more dominant at a probe temperature of 600 °C (Fig. 10b). The color code spectrum reinforces it with the highlight color on the Al element. In contrast to coal, palm fiber has smaller portions of Si, Al, and Fe but with a greater number of aggregated particles E, which are sticky and sintered during the deposition process, indicating that this sample is rich in Ca and K components [79].

For the palm leaves sample shown in Fig. 11, the ash sample at a probe temperature of 600 °C is dominated by particles A, supported by the EDS results, which show that the Si element has a portion of 30.1 wt%. However, similar to the palm fiber biomass sample, the palm leaves sample is also rich in Ca and K (particle E). Particle F in Fig. 11a represents unburned carbon with dark shapes that exist in the gaps of among other particles [80, 81]. These particles appear to be denser at a probe temperature of 550 °C than 600 °C. Carbon is not harmful to the formation of slagging

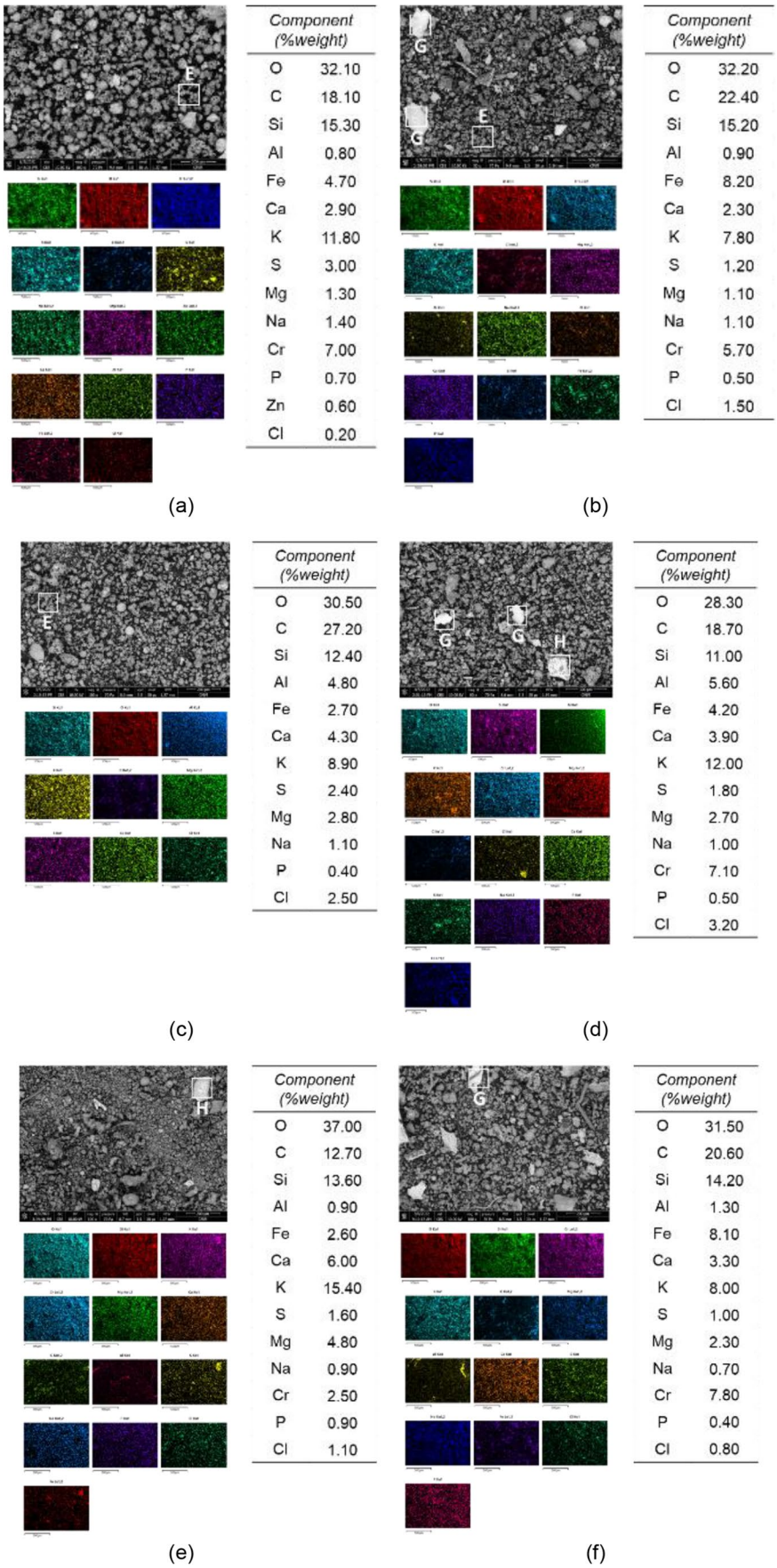

Fig. 12 Morphology and elemental analysis results of palm stem samples: (**a**) upper stem, probe temperature of 550 °C; (**b**) upper stem, probe temperature of 600 °C; (**c**) middle stem, probe temperature of 550 °C; (**d**) middle stem, probe temperature of 600 °C; (**e**) lower stem, probe temperature of 550 °C; and (**f**) lower stem, probe temperature of 600 °C

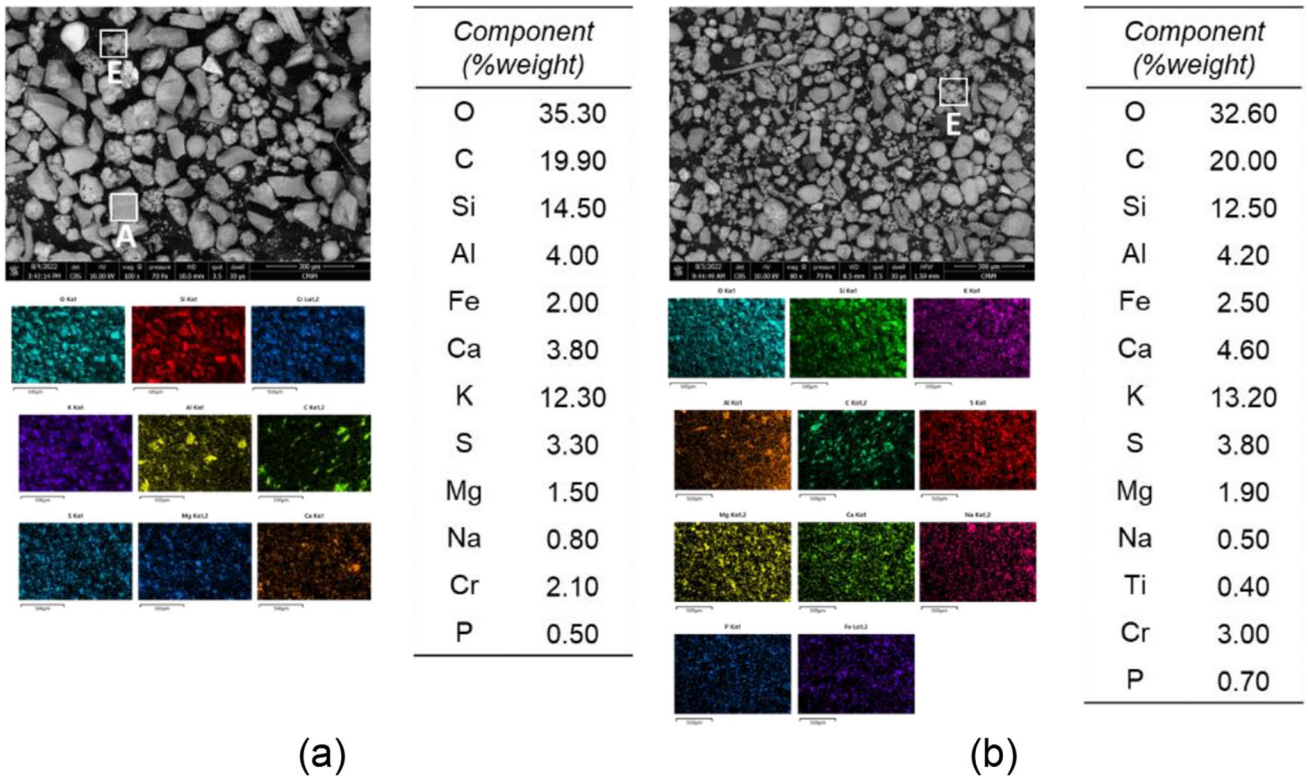

Component (%weight)	
O	35.30
C	19.90
Si	14.50
Al	4.00
Fe	2.00
Ca	3.80
K	12.30
S	3.30
Mg	1.50
Na	0.80
Cr	2.10
P	0.50

Component (%weight)	
O	32.60
C	20.00
Si	12.50
Al	4.20
Fe	2.50
Ca	4.60
K	13.20
S	3.80
Mg	1.90
Na	0.50
Ti	0.40
Cr	3.00
P	0.70

Fig. 13 Morphology and elemental analysis results of EFB samples: (**a**) probe temperature of 550 °C and (**b**) probe temperature of 600 °C

in the boiler, but it leads to higher emissions due to incomplete combustion [82, 83].

Figure 12 represents the SEM results of three different parts of the palm stem with probe temperatures of 550 and 600 °C, respectively. The morphology of all palm stems was dominated by particles E, rich in K, Ca, Na, S, and Mg. Ca, S, and Mg, which may adhere to other materials, leading to increased ash deposition in boilers [79]. In palm stem combustion, it was revealed that corrosion and erosion occurred, as evidenced by the presence of particles G in Fig. 11d with a very bright irregular shape indicating it is a heavy metal, which represents Cr in its color-coded spectrum. The presence of Cr in this sample is caused by the interaction between S, K, and Fe to form alkali sulfates [84] shown on particle H, with a similar morphology shape as particle G, making this component molten and reacting with stainless steel probe leading to corrosion and erosion, as shown from the probe observations in Fig. 6.

Figures 13 and 14 are EFB and palm frond samples whose morphological ash looks denser than other biomass samples. Particles contained in the EFB (see Fig. 13) appear to be dominated by particles with smooth surfaces (particle A) and aggregates of fine particles which sintered and adhered onto the surface of the coarse ash particles, which are dominated by element K and have a larger size estimated to be over 100 µm in size. In comparison, the particles contained in the palm frond are smaller in the 50–100-µm range. Smooth spherical ash particles (particle C) in Fig. 14 appear to have been molten during combustion. According to EDS results, these samples contained more Fe and O, indicating much iron oxide in the ash.

3.7 X-ray diffraction

XRD patterns are shown in Fig. 15a for the probe temperature of 550 °C and Fig. 15b for the probe temperature of 600 °C. At a probe temperature of 550 °C, coal contains 48.54 wt% albite ($NaAlSi_3O_8$), 47.25 wt% quartz (SiO_2), 2.18 wt% anhydrite ($CaSO_4$), and 2.03 wt% hematite (Fe_2O_3). A high percentage of albite must be considered because this mineral contains Na and has a melting point of 1118 °C. Albite here is formed because the high sulfur in coal reacts with alkaline Na to form Na_2SO_4. Furthermore, Na_2SO_4 reacts with aluminosilicate to form albite at temperatures above 575 °C [24]. Palm fiber has a high Na content resulting in high percentage of albite. Palm fiber at a probe temperature of 550 °C has 55.95 wt% albite, 14.20 wt% quartz, 14.03 wt% cristobalite (SiO_2), 8.88 wt% kumdykolite ($NaAlSi_3O_8$), 3.65 wt% calcite ($CaCO_3$), 3.07 wt% anhydrite, and 0.23 wt% hematite. Harmless minerals dominate palm leaves. Palm leaves at a probe temperature of 550 °C contain 93.88 wt% quartz, 2.12 wt% K_2CO_3, 2.04 wt% Ca, and 1.958 wt% hematite. Quartz

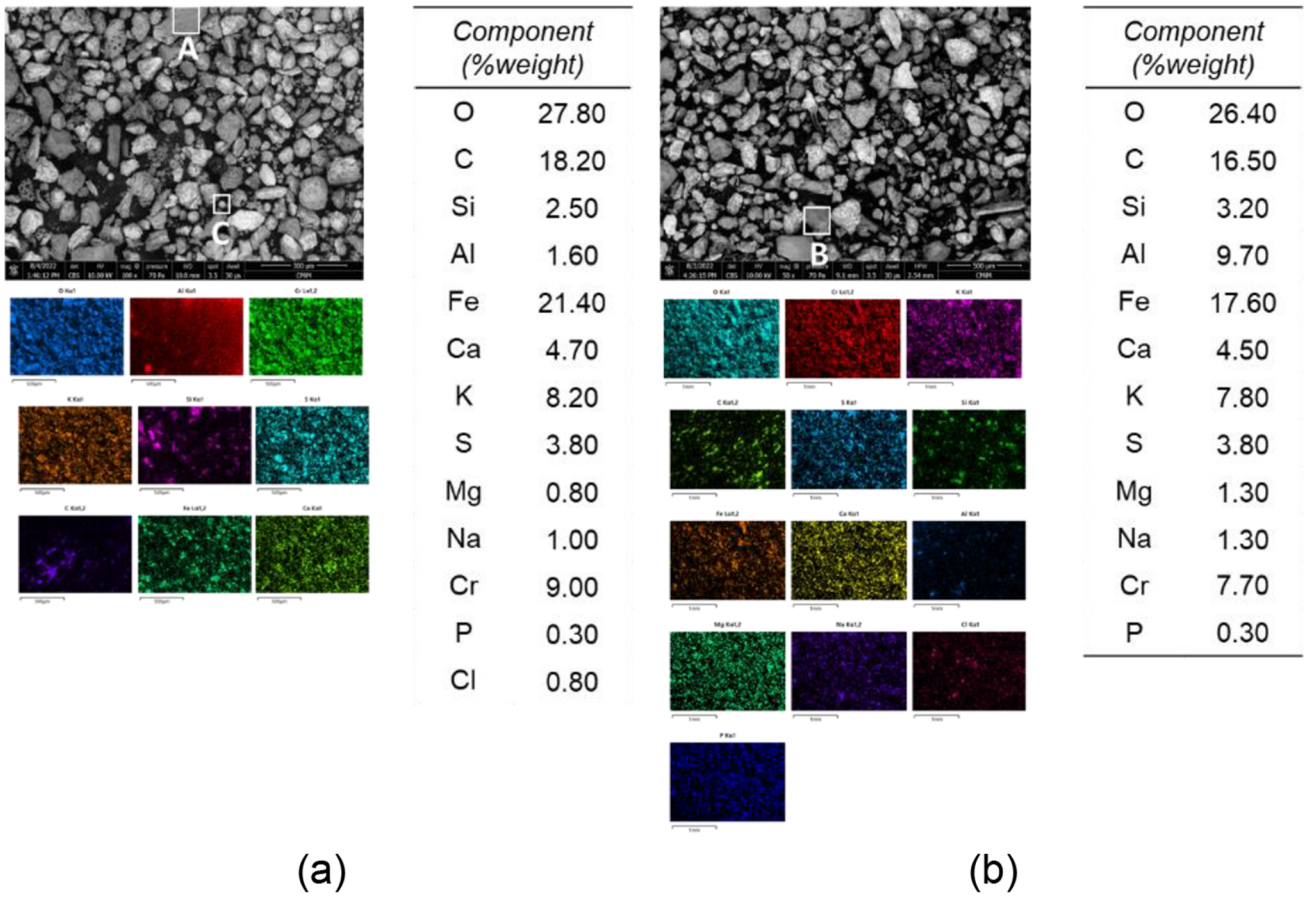

Component (%weight)	
O	27.80
C	18.20
Si	2.50
Al	1.60
Fe	21.40
Ca	4.70
K	8.20
S	3.80
Mg	0.80
Na	1.00
Cr	9.00
P	0.30
Cl	0.80

Component (%weight)	
O	26.40
C	16.50
Si	3.20
Al	9.70
Fe	17.60
Ca	4.50
K	7.80
S	3.80
Mg	1.30
Na	1.30
Cr	7.70
P	0.30

Fig. 14 Morphology and elemental analysis results of palm frond samples: (**a**) probe temperature of 550 °C and (**b**) probe temperature of 600 °C

dominates palm leaves with a melting point of 1730 °C [24, 61, 68], which may contribute to the increased AFT of palm leaves. Interestingly, each part of the palm stem at a probe temperature of 550 °C has different mineral constituents. The upper stem has 88.40 wt% diopside ($MgCaSi_2O_6$), 4.82 wt% quartz, 5.43 wt% moganite (SiO_2), 0.41 wt% sylvite (KCl), and 0.95 wt% hematite. This upper stem is dominated by diopside with a melting point of 1391 °C [85, 86]. Harmful minerals dominate the middle stem where the mineral consists of 28.77 wt% sylvite, 26.47 wt% aphthitalite ($K_3Na(SO_4)_2$), 23.00 wt% quartz, 5.18 wt% $FePO_4$, 4.78 wt% anhydrite, 4.66 wt% $Mg_2P_2O_7$, 3.75 wt% hematite, 2.63 wt% MgO, and 0.78 wt% magnesioferrite ($MgFe_2O_4$). Sylvite and aphthitalite are harmful because of potassium and sodium content that may contribute to slagging and fouling [29]. In addition, sylvite melts at a temperature of 770–790 °C [24, 87, 88], and chlorine in sylvite also has a negative effect on corrosion [89]. The lower stem has 40.73 wt% hematite, 19.31 wt% arcanite (K_2SO_4), 19.26 wt% magnesioferrite, 5.56 wt% quartz, 5.55 wt% $FePO_4$, 4.08 wt% anhydrite, 3.28 wt% Ca, and 2.24 wt% $Ca_2Fe_2O_5$. Arcanite, $FePO_4$, Ca, and $Ca_2Fe_2O_5$ have a low melting point below 1250 °C [68, 90, 91]. Although more than 20 wt% of minerals in the lower stem have a low melting point, this lower stem is still dominated by harmless minerals with a high melting point higher than 1350 °C such as hematite, magnesioferrite, quartz, and anhydrite [24, 61, 68, 92]. Then, EFB at a probe temperature of 550 °C contains 53.78 wt% albite, 40.82 wt% quartz, 2.73 wt% calcite, 1.59 wt% hematite, and 1.08 wt% cristobalite. As mentioned before, the domination of albite in EFB may have a negative effect because of sodium content and its low melting point. Meanwhile, palm frond is dominated by harmless minerals such as hematite and clinoenstatite ($MgSiO_3$) that possibly melt at a temperature of higher than 1350 °C [24, 93, 94]. This palm frond comprises 61.75 wt% hematite, 29.21 wt% clinoenstatite, 5.13 wt% magnesioferrite, 1.78 wt% S_8, 1.29 wt% quartz, and 0.85 wt% calcite.

As shown in Fig. 10b, there is no significant difference between the XRD results of probe temperature of 550 °C. Coal and palm fiber also contain a high percentage of albite. Coal has 48.66 wt% albite, 46.93 wt% quartz, 2.24 wt% anhydrite, and 2.17 wt% hematite. Palm fiber contains 49.24 wt% albite, 23.63 wt% quartz, 21.16 wt% cristobalite, 4.14 wt% calcite, and 1.84 wt% hematite.

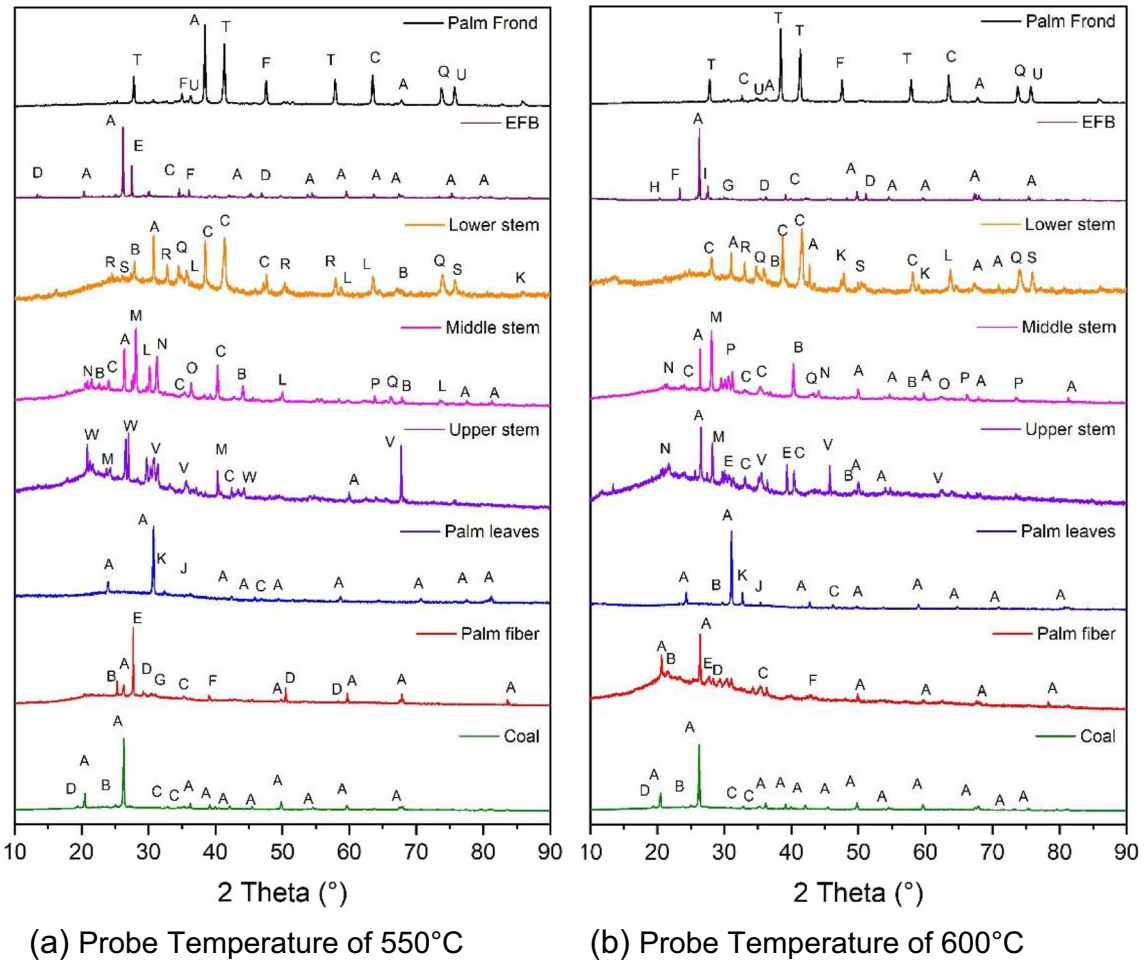

Fig. 15 XRD plotting diagram of coal and biomass samples: (A) quartz; (B) anhydrite; (C) hematite; (D) albite; (E) cristobalite; (F) calcite; (G) kumdykolite; (H) berlinite; (I) SO_3; (J) K_2CO_3; (K) Ca; (L) $FePO_4$; (M) sylvite; (N) aphthitalite; (O) MgO; (P) $Mg_2P_2O_7$; (Q) magnesioferrite; (R) arcanite; (S) $Ca_2Fe_2O_5$; (T) clinoenstatite; (U) S_8; (V) diopside; (W) moganite

At a probe temperature of 600 °C, palm leaves are also dominated by harmless minerals containing 86.81 wt% quartz, 4.395 wt% anhydrite, 3.76 wt% K_2CO_3, 3.67 wt% Ca, and 1.36 wt% hematite. Similar to the probe temperature of 550 °C, each side of the palm stem has different mineral constituents at a probe temperature of 600 °C. The upper stem contains 29.96 wt% quartz, 26.70 wt% diopside, 18.34 wt% cristobalite, 9.66 wt% sylvite, 9.47 wt% hematite, 3.85 wt% aphthitalite, and 2.03 wt% anhydrite. This upper stem is still dominated by harmless minerals such as quartz, diopside, and cristobalite. As mentioned, quartz and diopside have melting points at 1730 and 1391 °C, respectively, while cristobalite melts at 1730 °C [61]. Harmful minerals also dominate the middle stem with 24.48 wt% sylvite, 18.87 wt% $FePO_4$, 14.93 wt% $Mg_2P_2O_7$, 12.34 wt% aphthitalite, 5.65 wt% magnesioferrite, 5.35 wt% hematite, 3.93 wt% MgO, and 2.90 wt% anhydrite. As mentioned before, sylvite and aphthitalite have a negative effect due to the content of potassium, sodium, and total chlorine [29, 89]. Moreover, $FePO_4$ melts at below 1000 °C [91], which may trigger the melting ash. Lower stem at a probe temperature of 600 °C is still dominated by harmless minerals even though it contains more than 20 wt% harmful minerals such as arcanite, $Ca_2Fe_2O_5$, $FePO_4$, and Ca. The lower stem contains 42.70 wt% hematite, 18.08 wt% magnesioferrite, 15.69 wt% quartz, 13.48 wt% arcanite, 3.32 wt% $Ca_2Fe_2O_5$, 2.49 wt% anhydrite, 2.13 wt% $FePO_4$, and 2.09 wt% Ca. EFB at probe temperature of 600 °C consists of 51.10 wt% quartz, 21.09 wt% kumdykolite, 14.58 wt% SO_3, 5.87 wt% albite, 3.69 wt% berlinite, 1.89 wt% calcite, and 1.79 wt% hematite. Kumdykolite is a polymorph of albite [95–98, 98]. As mentioned before, albite may trigger the problem of slagging and fouling because of its low melting point and sodium content. SO_3 also has a negative effect related to corrosion because it can react with other elements forming HCl and H_2S in the gas phase [89, 99]. Similar to a probe temperature of 550 °C, the palm frond at a probe temperature of 600 °C is

also dominated by harmless minerals such as hematite and clinoenstatite. Palm frond contains 64.30 wt% hematite, 30.04 wt% clinoenstatite, 2.21 wt% magnesioferrite, 1.52 wt% S_8, 1.35 wt% quartz, and 0.57 wt% calcite.

4 Discussion

Coal is used as a baseline for comparison of combustion for other oil palm waste biomass because it has good combustion characteristics supported with a calorific that is suitable as the main fuel for the pulverized fuel boiler. Probe observations produced by coal are also relatively clean without adhered ash on the probe's surface. SEM-EDS and XRD analyses also show that coal was dominated by high Si and Al.

The high volatility of oil palm wastes causes various ash components and may increase the slagging and fouling potential during combustion. It can be observed that palm fiber has combustion characteristics similar and close to coal, indicated by the consistency of slagging and fouling prediction calculations, calorific values, AFTs, and several combustion characteristics from TGA analysis, such as T_{ig}, T_{bo}, and T_{max}. However, palm fiber has sintered ash particles in probe observation and further confirmed by K-based minerals such as albite are found in relatively high amounts. Palm leaves with a less prominent ash component, but still high in SiO_2 and Al_2O_3, produce the highest AFT among other palm biomass. The SEM-EDS and XRD analysis results show that Si dominates the palm leaves ash in the form of quartz with high melting temperatures.

EFB, which is rich in potassium, has a high slagging tendency. This is supported by the results of ash mineralogy analysis using SEM and XRD, where mineral albite with low melting point predominates. However, it has cleaner probe observations and lower ash deposits, which can be an added value for EFB. Palm frond is rich in iron content, producing 28.59 wt% Fe_2O_3 in ash analysis, corroborated by the results of combustion ash with higher Fe and mineral hematite contents in the SEM and XRD results. Iron has a low melting point and easily reacts to other components, such as S and Cl, producing FeS2 and FeCl2, which leads to slagging and corrosion [24].

From probe observation, palm stems with a high chlorine value show a higher corrosion tendency. As proven by SEM-EDS analysis, Cr elements were carried away when the ashes were brushed from the probe. This shows that the palm stems corrosiveness can peel off the outer layer of steel. Moreover, Fe-based and alkali-based minerals are observed in XRD analysis. In addition, palm stems also have higher ash deposits due to the domination of low-melting alkali-based minerals and bright particles that indicate heavy metals in the ash mineralogy results [79, 100].

5 Conclusions

Based on a series of analyses that have been carried out to investigate the oil palm waste biomass in the combustion aspect as single fuel, it can be concluded that each type of oil palm waste biomass has different characteristics. Palm fiber has the highest calorific value among oil palm wastes and similar combustion characteristics to coal, but it has sintered ash particles attached to the surface of the probe. Palm leaves, EFB, and palm fronds have relatively clean probe observation; however, it needs to consider K-based and Fe-based minerals that can be formed. On the other hand, palm stems with high chlorine content increase the tendency of corrosion during combustion. According to this study, palm leaves, EFB, and palm fronds can be recommended to be utilized as biomass fuel for co-firing. However, further investigation on co-firing between oil palm wastes, coal, or other solid fuel is recommended to find the compatibility and blend composition for optimal combustion and mitigate ash-related problems.

Author contribution Fairuz Milkiy Kuswa: data curation, writing – original draft, investigation. Hanafi Prida Putra: data curation, writing, editing. Prabowo: conceptualization, supervision, methodology. Arif Darmawan: data curation, writing, editing. Muhammad Aziz: supervision, writing, editing. Hariana: conceptualization, writing, methodology, supervision.

Funding Open access funding is provided by The University of Tokyo.

Data availability Data will be made available on request

Declarations

Ethical approval This material is the authors' own original work, which has not been previously published elsewhere. The paper is not currently being considered for publication elsewhere.

This paper does not contain any data taken directly from any published article.
This research did not contain any studies involving animal or human participants, nor did it take place in any private or protected areas. No specific permissions were required for corresponding locations.

Competing interests The authors declare no competing interests.

References

1. Borowski PF (2022) Mitigating climate change and the development of green energy versus a return to fossil fuels due to the energy crisis in 2022. Energies 15:9289
2. Xu Y, Yang K, Zhou J, Zhao G (2020) Coal-biomass co-firing power generation technology: current status, challenges and policy implications. Sustainability 12:3692. https://doi.org/10.3390/su12093692
3. Wu X, Wu K, Zhang Y et al (2017) Comparative life cycle assessment and economic analysis of typical flue-gas cleaning processes of coal-fired power plants in China. J Clean Prod 142:3236–3242. https://doi.org/10.1016/j.jclepro.2016.10.146
4. Paraschiv S, Paraschiv LS (2020) Trends of carbon dioxide (CO2) emissions from fossil fuels combustion (coal, gas and oil) in the EU member states from 1960 to 2018. Energy Reports 6:237–242. https://doi.org/10.1016/j.egyr.2020.11.116
5. Zapata-mina J, Restrepo A, Esteban J (2023) Case studies in thermal engineering assessment of the exergy , emissions , and combustion characteristics of a diesel engine operating on low-glyceride biodiesel blended with diesel fuel. Case Stud Therm Eng 41. https://doi.org/10.1016/j.csite.2022.102636
6. Edenhofer O, Steckel JC, Jakob M, Bertram C (2018) Reports of coal's terminal decline may be exaggerated. Environ Res Lett 13. https://doi.org/10.1088/1748-9326/aaa3a2
7. Yang Q, Zhou H, Bartocci P et al (2021) Prospective contributions of biomass pyrolysis to China's 2050 carbon reduction and renewable energy goals. Nat Commun 12:1–12. https://doi.org/10.1038/s41467-021-21868-z
8. Rehfeldt M, Worrell E, Eichhammer W, Fleiter T (2020) A review of the emission reduction potential of fuel switch towards biomass and electricity in European basic materials industry until 2030. Renew Sust Energ Rev 120:109672. https://doi.org/10.1016/j.rser.2019.109672
9. Deng L, Jin X, Long J, Che D (2019) Ash deposition behaviors during combustion of raw and water washed biomass fuels. J Energy Inst 92:959–970. https://doi.org/10.1016/j.joei.2018.07.009
10. Rosendahl L (2013) Biomass combustion science, technology and engineering. Woodhead Publishing, London
11. Alami AH, Tawalbeh M, Alasad S et al (2021) Cultivation of *Nannochloropsis* algae for simultaneous biomass applications and carbon dioxide capture. Energ Source Part A:1–12. https://doi.org/10.1080/15567036.2021.1933267
12. Verma M, Loha C, Sinha AN, Chatterjee PK (2017) Drying of biomass for utilising in co-firing with coal and its impact on environment – a review. Renew Sust Energ Rev 71:732–741. https://doi.org/10.1016/j.rser.2016.12.101
13. Loo S van, Koppejan J (2008) The handbook of biomass combustion and co-firing. Antony Rowe, Chippenham, London
14. Index Mundi (2022) Palm oil production by country in 1000 MT. https://www.indexmundi.com/agriculture/?commodity=palm-oil. Accessed 10 Oct 2022
15. Hariana P, Hilmawan E et al (2023) A comprehensive evaluation of co-firing biomass with coal and slagging-fouling tendency in pulverized coal-fired boilers. Ain Shams Eng J 14(7):102001. https://doi.org/10.1016/j.asej.2022.102001
16. Darmawan A, Asyhari T, Dunggio I et al (2023) Energy harvesting from tropical biomasses in Wallacea region: scenarios, technologies, and perspectives. Biomass Convers Biorefin. https://doi.org/10.1007/s13399-023-04223-8
17. Hamada HM, Al-Attar A, Shi J et al (2023) Optimization of sustainable concrete characteristics incorporating palm oil clinker and nano-palm oil fuel ash using response surface methodology. Powder Technol 413:118054. https://doi.org/10.1016/j.powtec.2022.118054
18. Hamada HM, Shi J, Abed F et al (2023) Recycling solid waste to produce eco-friendly ultra-high performance concrete: a review of durability, microstructure and environment characteristics. Sci Total Environ 876:162804. https://doi.org/10.1016/j.scitotenv.2023.162804
19. Salleh SF, Abd Rahman A, Abdullah TART (2018) Potential of deploying empty fruit bunch (EFB) for biomass co-firing in Malaysia's largest coal power plant. 2018 IEEE 7th Int Conf Power Energy. PECon 2018:429–433. https://doi.org/10.1109/PECON.2018.8684124
20. Up O, Ko O, Owamah HI, Ci S, Adingwupu AC (2022) Assessment of power generation potential from the co-firing of Elaeis Guineensis Residues with coal pellets in a popular Nigerian palm oil research institute. Int J Coal Prep Util 42:2804–2819. https://doi.org/10.1080/19392699.2021.1908272
21. Mohd Idris MN, Hashim H (2021) Integrating palm oil biomass waste utilization in coal-fired power plants for meeting near-term emission targets. J Environ Manage 296:113118. https://doi.org/10.1016/j.jenvman.2021.113118
22. Vassilev SV, Vassileva CG, Song Y-C et al (2017) Ash contents and ash-forming elements of biomass and their significance for solid biofuel combustion. Fuel 208:377–409. https://doi.org/10.1016/j.fuel.2017.07.036
23. Putra HP, Hilmawan E, Darmawan A et al (2023) Theoretical and experimental investigation of ash-related problems during coal co-firing with different types of biomass in a pulverized coal-fired boiler. Energy 269:126784. https://doi.org/10.1016/j.energy.2023.126784
24. Vassilev SV, Baxter D, Vassileva CG (2013) An overview of the behaviour of biomass during combustion: Part I. Phase-mineral transformations of organic and inorganic matter. Fuel 112:391–449. https://doi.org/10.1016/j.fuel.2013.05.043
25. Madejski P, Janda T, Taler J et al (2018) Analysis of fouling degree of individual heating surfaces in a pulverized coal fired boiler. J Energy Resour Technol Trans ASME 140:1–8. https://doi.org/10.1115/1.4037936
26. Chen C, Bi Y, Huang Y, Huang H (2021) Review on slagging evaluation methods of biomass fuel combustion. J Anal Appl Pyrolysis 155:105082. https://doi.org/10.1016/j.jaap.2021.105082
27. Oladejo JM, Adegbite S, Pang C et al (2020) In-situ monitoring of the transformation of ash upon heating and the prediction of ash fusion behaviour of coal/biomass blends. Energy 199:117330. https://doi.org/10.1016/j.energy.2020.117330
28. Qian X, Xue J, Yang Y, Lee SW (2021) Thermal properties and combustion-related problems prediction of agricultural crop residues. Energies 14. https://doi.org/10.3390/en14154619
29. Li N, Vainio E, Hupa L et al (2018) Interaction of high Al2O3 refractories with alkaline salts containing potassium and sodium in biomass and waste combustion. Energ Fuel 32:12971–12980. https://doi.org/10.1021/acs.energyfuels.8b03136
30. Yacob NS, Mohamed H, Shamsuddin AH (2021) Investigation of palm oil wastes characteristics for co-firing with coal. J Adv Res Appl Sci Eng Technol 23:34–42. https://doi.org/10.37934/araset.23.1.3442
31. Niu Y, Tan H, Wang X et al (2010) Study on fusion characteristics of biomass ash. Bioresour Technol 101:9373–9381. https://doi.org/10.1016/j.biortech.2010.06.144
32. Putra HP, Karuana F, Ruhiyat AS et al (2022) Effect of MgO-based additive on the sintering behavior for slagging-fouling mitigation in Indonesian coal combustion. Int J Coal Prep Util 1–11. https://doi.org/10.1080/19392699.2022.2118257
33. Liang W, Wang G, Ning X et al (2020) Application of BP neural network to the prediction of coal ash melting characteristic

temperature. Fuel 260:116324. https://doi.org/10.1016/j.fuel.2019.116324
34. Lachman J, Baláš M, Lisý M et al (2021) An overview of slagging and fouling indicators and their applicability to biomass fuels. Fuel Process Technol 217:106804. https://doi.org/10.1016/J.FUPROC.2021.106804
35. Kitto JB, Stultz SC (2005) Steam: its generation and use, 41st edn. Barberton, OH (United States)
36. Raask E (1985) Mineral impurities in coal combustion: behavior, problems, and remedial measures. Hemisphere Publishing Corporation, Washington, DC, United States
37. Zhu C, Tu H, Bai Y et al (2019) Evaluation of slagging and fouling characteristics during Zhundong coal co-firing with a Si/Al dominated low rank coal. Fuel 254. https://doi.org/10.1016/j.fuel.2019.115730
38. Jeong T-Y, Sh L, Kim J-H et al (2019) Experimental investigation of ash deposit behavior during co-combustion of bituminous coal with wood pellets and empty fruit bunches. Energies 12:2087
39. Garcia-Maraver A, Mata-Sanchez J, Carpio M, Perez-Jimenez JA (2017) Critical review of predictive coefficients for biomass ash deposition tendency. J Energy Inst 90:214–228. https://doi.org/10.1016/j.joei.2016.02.002
40. Ghazidin H, Prayoga MZE, Putra HP et al (2023) A comprehensive evaluation of slagging and fouling indicators for solid fuel combustion. Therm Sci Eng Prog 40:101769. https://doi.org/10.1016/j.tsep.2023.101769
41. Hariana PA, Ahmadi GA, Darmawan A (2021) Ash evaluation of indonesian coal blending for pulverized coal-fired boilers. J Combust 2021. https://doi.org/10.1155/2021/8478739
42. Wang C, Sun R, Zhao L et al (2020) Experimental study on fouling and slagging behaviors during oxy-fuel combustion of high-sodium coal using a high-temperature drop-tube furnace. Int J Greenh Gas Control 97:103054. https://doi.org/10.1016/j.ijggc.2020.103054
43. Sahu SG, Sarkar P, Chattopadhyay US et al (2019) Investigation on the combustion behavior of coal at various level of washing in TGA and drop tube furnace. Trans Indian Ceram Soc 78:181–186. https://doi.org/10.1080/0371750X.2019.1668853
44. Li S, Xu T, Sun P et al (2008) NOx and SOx emissions of a high sulfur self-retention coal during air-staged combustion. Fuel 87:723–731. https://doi.org/10.1016/j.fuel.2007.05.043
45. Öhman M, Boman C, Hedman H et al (2004) Slagging tendencies of wood pellet ash during combustion in residential pellet burners. Biomass Bioenergy 27:585–596. https://doi.org/10.1016/j.biombioe.2003.08.016
46. Kutchko BG, Kim AG (2006) Fly ash characterization by SEM-EDS. Fuel 85:2537–2544. https://doi.org/10.1016/j.fuel.2006.05.016
47. Kozlov A, Svishchev D, Donskoy I et al (2015) A technique proximate and ultimate analysis of solid fuels and coal tar. J Therm Anal Calorim 122:1213–1220. https://doi.org/10.1007/s10973-015-5134-7
48. Kosugi A, Tanaka R, Magara K et al (2010) Ethanol and lactic acid production using sap squeezed from old oil palm trunks felled for replanting. J Biosci Bioeng 110:322–325. https://doi.org/10.1016/j.jbiosc.2010.03.001
49. Heinzel T, Siegle V, Spliethoff H, Hein KRG (1998) Investigation of slagging in pulverized fuel co-combustion of biomass and coal at a pilot-scale test facility. Fuel Process Technol 54:109–125. https://doi.org/10.1016/S0378-3820(97)00063-5
50. Rushdi A, Sharma A, Gupta R (2004) An experimental study of the effect of coal blending on ash deposition. Fuel 83:495–506. https://doi.org/10.1016/j.fuel.2003.08.013
51. Hu J, Yan Y, Song Y et al (2020) Catalytic combustions of two bamboo residues with sludge ash, CaO, and Fe2O3: bioenergy, emission and ash deposition improvements. J Clean Prod 270:122418. https://doi.org/10.1016/j.jclepro.2020.122418
52. Niu Y, Tan H, Hui S (2016) Ash-related issues during biomass combustion: alkali-induced slagging, silicate melt-induced slagging (ash fusion), agglomeration, corrosion, ash utilization, and related countermeasures. Prog Energy Combust Sci 52:1–61. https://doi.org/10.1016/j.pecs.2015.09.003
53. Zi J, Ma D, Wang X et al (2020) Slagging behavior and mechanism of high-sodium–chlorine coal combustion in a full-scale circulating fluidized bed boiler. J Energy Inst 93:2264–2270. https://doi.org/10.1016/j.joei.2020.06.009
54. Nunes LJR, Matias JCO, Catalão JPS (2016) Biomass combustion systems: a review on the physical and chemical properties of the ashes. Renew Sust Energ Rev 53:235–242. https://doi.org/10.1016/j.rser.2015.08.053
55. Wang C, Tang G, Sun R et al (2020) The correlations of chemical property, alkali metal distribution, and fouling evaluation of Zhundong coal. J Energy Inst 93:2204–2214. https://doi.org/10.1016/j.joei.2020.06.002
56. Prismantoko A, Hilmawan E, Darmawan A, Aziz M (2023) Effectiveness of different additives on slagging and fouling tendencies of blended coal. J Energy Inst 107:101192. https://doi.org/10.1016/j.joei.2023.101192
57. Zevenhoven M, Yrjas P, Skrifvars B-J, Hupa M (2012) Characterization of ash-forming matter in various solid fuels by selective leaching and its implications for fluidized-bed combustion. Energ Fuel 26:6366–6386
58. Wang Y, Xiang Y, Wang D et al (2016) Effect of sodium oxides in ash composition on ash fusibility. Energ Fuel 30:1437–1444. https://doi.org/10.1021/acs.energyfuels.5b02722
59. Wei B, Wu W, Liu K et al (2020) Investigation of slagging characteristics on middle and low temperature heat transfers by burning high sodium and iron coal. Combust Sci Technol 194:1768–1787. https://doi.org/10.1080/00102202.2020.1830768
60. Akiyama K, Pak H, Ueki Y et al (2011) Effect of MgO addition to upgraded brown coal on ash-deposition behavior during combustion. Fuel 90:3230–3236. https://doi.org/10.1016/j.fuel.2011.06.041
61. He C, Bai J, Ilyushechkin A et al (2019) Effect of chemical composition on the fusion behaviour of synthetic high-iron coal ash. Fuel 253:1465–1472. https://doi.org/10.1016/j.fuel.2019.05.135
62. Li F, Fan H, Fang Y (2017) Investigation on the regulation mechanism of ash fusion characteristics in coal blending. Energ Fuel 31:379–386. https://doi.org/10.1021/acs.energyfuels.6b02539
63. Vassilev SV, Baxter D, Vassileva CG (2014) An overview of the behaviour of biomass during combustion: Part II. Ash fusion and ash formation mechanisms of biomass types. Fuel 117:152–183. https://doi.org/10.1016/j.fuel.2013.09.024
64. Hare N, Rasul M, Moazzem S (2010) A review on boiler deposition/foulage prevention and removal techniques for power plant. In: Recent Advances in Energy and Environment. Proceedings of the 5th IASME/WSEAS International Conference on Energy & Enviroment (EE'10. vol 23. World Scientific and Engineering Academy and Society (WSEAS) Stevens Point, Wisconsin, United States, p 25
65. Yan Y, Meng Y, Tang L et al (2019) Ignition and kinetic studies: the influence of lignin on biomass combustion. Energ Fuel 33:6463–6472. https://doi.org/10.1021/acs.energyfuels.9b01089
66. Umar DF, Suganal S, Monika I et al (2020) The influence of steam drying process on combustion behavior of Indonesian low-rank coals. Indones Min J 23:105–115
67. Marinov SP, Gonsalvesh L, Stefanova M et al (2010) Combustion behaviour of some biodesulphurized coals assessed by TGA/

DTA. Thermochim Acta 497:46–51. https://doi.org/10.1016/j.tca.2009.08.012
68. Vamvuka D, Panagopoulos G, Sfakiotakis S (2020) Investigating potential co-firing of corn cobs with lignite for energy production. Thermal analysis and behavior of ashes. Int J Coal Prep Util 00:1–12. https://doi.org/10.1080/19392699.2020.1856099
69. Lindström E, Sandström M, Boström D, Öhman M (2007) Slagging characteristics during combustion of cereal grains rich in phosphorus. Energ Fuel 21:710–717. https://doi.org/10.1021/ef060429x
70. Liu Y, Cheng L, Ji J, Zhang W (2019) Ash deposition behavior in co-combusting high-alkali coal and bituminous coal in a circulating fluidized bed. Appl Therm Eng 149:520–527. https://doi.org/10.1016/j.applthermaleng.2018.12.080
71. Yan T, Bai J, Kong L et al (2017) Effect of SiO2/Al2O3 on fusion behavior of coal ash at high temperature. Fuel 193:275–283
72. Hariana GH, Putra HP et al (2023) The effects of additives on deposit formation during co-firing of high-sodium coal with high-potassium and -chlorine biomass. Energy 271:127096. https://doi.org/10.1016/j.energy.2023.127096
73. Lin X, Yang Y, Yang S et al (2016) Initial deposition feature during high-temperature pressurized pyrolysis of a typical Zhundong coal. Energ Fuel 30:6330–6341. https://doi.org/10.1021/acs.energyfuels.6b01074
74. Kim JH, Lee YJ, Yu J, Jeon CH (2019) Improvement in reactivity and pollutant emission by co-firing of coal and pretreated biomass. Energ Fuel 33:4331–4339. https://doi.org/10.1021/acs.energyfuels.9b00396
75. Lin Y, Ma X, Ning X, Yu Z (2015) TGA-FTIR analysis of co-combustion characteristics of paper sludge and oil-palm solid wastes. Energy Convers Manag 89:727–734. https://doi.org/10.1016/j.enconman.2014.10.042
76. Ren X, Sun R, Meng X et al (2017) Carbon, sulfur and nitrogen oxide emissions from combustion of pulverized raw and torrefied biomass. Fuel 188:310–323. https://doi.org/10.1016/j.fuel.2016.10.017
77. Yanik J, Duman G, Karlström O, Brink A (2018) NO and SO2 emissions from combustion of raw and torrefied biomasses and their blends with lignite. J Environ Manage 227:155–161. https://doi.org/10.1016/j.jenvman.2018.08.068
78. Fisher GL, Prentice BA, Sllberman D et al (1978) Physical and morphological studies of size-classified coal fly ash. Environ Sci Technol 12:447–451. https://doi.org/10.1021/es60140a008
79. Li J, Zhu M, Zhang Z et al (2016) Characterisation of ash deposits on a probe at different temperatures during combustion of a Zhundong lignite in a drop tube furnace. Fuel Process Technol 144:155–163. https://doi.org/10.1016/j.fuproc.2015.12.024
80. Bailey JG, Tate A, Diessel CFK, Wall TF (1990) A char morphology system with applications to coal combustion. Fuel 69:225–239. https://doi.org/10.1016/0016-2361(90)90179-T
81. Mishra SB, Langwenya SP, Mamba BB, Balakrishnan M (2010) Study on surface morphology and physicochemical properties of raw and activated South African coal and coal fly ash. Phys Chem Earth 35:811–814. https://doi.org/10.1016/j.pce.2010.07.001
82. Bartoňová L (2015) Unburned carbon from coal combustion ash: an overview. Fuel Process Technol 134:136–158. https://doi.org/10.1016/j.fuproc.2015.01.028
83. Rybak W, Moroń W, Czajka KM et al (2017) Co-combustion of unburned carbon separated from lignite fly ash. Energy Procedia 120:197–205. https://doi.org/10.1016/j.egypro.2017.07.165
84. Natesan K, Purohit A, Rink DL (2003) Coal-ash corrosion of alloys for combustion power plants. In: Proc 17th Annu Conf Foss Energy Mater April 22-24, 2003. Argonne National Lab., Argonne, IL (US), pp 1–15
85. Guo S, Gao J, Zhao D et al (2022) Co-combustion of sewage sludge and Zhundong coal: Effects of combustion conditions on gaseous pollutant emission and ash properties. Sustain Energy Technol Assess 54:102836. https://doi.org/10.1016/j.seta.2022.102836
86. Choudhary R, Venkatraman SK, Bulygina I et al (2021) Biomineralization, dissolution and cellular studies of silicate bioceramics prepared from eggshell and rice husk. Mater Sci Eng C 118:111456. https://doi.org/10.1016/j.msec.2020.111456
87. Fan H, Li F, Guo Q, Guo M (2021) Effect of biomass ash on initial sintering and fusion characteristics of high melting coal ash. J Energy Inst 94:129–138. https://doi.org/10.1016/j.joei.2020.11.008
88. Yao X, Zhou H, Xu K et al (2019) Evaluation of the fusion and agglomeration properties of ashes from combustion of biomass, coal and their mixtures and the effects of K2CO3 additives. Fuel 255. https://doi.org/10.1016/j.fuel.2019.115829
89. Míguez JL, Porteiro J, Behrendt F et al (2021) Review of the use of additives to mitigate operational problems associated with the combustion of biomass with high content in ash-forming species. Renew Sust Energ Rev 141:110502
90. Barbosa MM, Puschmann R, Thiele S et al (2014) Development of thermally sprayed Ca2Fe2O5 coatings for thermoelectrical applications. Proc ITSC 2014:485–490
91. Lajmi B, Hidouri M, Rzeigui M, Ben Amara M (2002) Synthesis and crystal structure of a new magnesium phosphate Na3RbMg7(PO4)6. Mater Res Bull 37:2407–2416. https://doi.org/10.1107/S2056989017006363
92. Xue P, He D, Xu A et al (2017) Modification of industrial BOF slag: formation of MgFe2O4 and recycling of iron. J Alloys Compd 712:640–648. https://doi.org/10.1016/j.jallcom.2017.04.142
93. Qu Y, Yang Y, Zou Z et al (2015) Melting and reduction behaviour of individual fine hematite ore particles. ISIJ Int 55:149–157. https://doi.org/10.2355/isijinternational.55.149
94. Gu F, Peng Z, Tang H et al (2018) Preparation of refractory materials from ferronickel slag. Miner Met Mater Ser Part F8:633–642. https://doi.org/10.1007/978-3-319-72484-3_67
95. Borghini A, Ferrero S, O'Brien PJ et al (2020) Cryptic metasomatic agent measured in situ in Variscan mantle rocks: melt inclusions in garnet of eclogite, Granulitgebirge, Germany. J Metamorph Geol 38:207–234. https://doi.org/10.1111/jmg.12519
96. Ferrero S, Ziemann MA, Angel RJ et al (2016) Kumdykolite, kokchetavite, and cristobalite crystallized in nanogranites from felsic granulites, Orlica-Snieznik Dome (Bohemian Massif): not an evidence for ultrahigh-pressure conditions. Contrib to Mineral Petrol 171:1–12. https://doi.org/10.1007/s00410-015-1220-x
97. Hwang S-LS, Chu H-TY, Sobolev NV (2010) Kumdykolite, an orthorhombic polymorph of albite, from the Kokchetav ultrahigh-pressure massif, Kazakhstan. Eur J Mineral 21:1325–1334. https://doi.org/10.1127/0935-1221/2009/0021-1970
98. Schönig J, von Eynatten H, Meinhold G et al (2020) Deep subduction of felsic rocks hosting UHP lenses in the central Saxonian Erzgebirge: implications for UHP terrane exhumation. Gondwana Res 87:320–329. https://doi.org/10.1016/j.gr.2020.06.020
99. Bryers RW (1996) Fireside slagging, fouling, and high-temperature corrosion of heat-transfer surface due to impurities in steam-raising fuels. Prog Energy Combust Sci 22:29–120. https://doi.org/10.1016/0360-1285(95)00012-7
100. Luan C, You C, Zhang D (2014) Composition and sintering characteristics of ashes from co- fi ring of coal and biomass in a laboratory-scale drop tube furnace. Energy 1–9. https://doi.org/10.1016/j.energy.2014.03.050